ON SUBHARMONIC INSTABILITY IN BOUNDARY LAYERS

by

Jamal Masad

Thesis submitted to the Faculty of the

Virginia Polytechnic Institute and State University

in partial fulfillment of the requirements for the degree of

MASTER OF SCIENCE

in

Engineering Mechanics

APPROVED:

Ali H. Nayfeh, Chairman

Dean T. Mook

Saad A. Ragab

December 1987

Blacksburg, Virginia

ACKNOWLEDGEMENTS

At the top of the list of gratitude is Dr. Ali H. Nayfeh. Without his supervision this work would not have materialized. Thanks are given also to Drs. D. T. Mook and S. A. Ragab for their contribution as committee members.

I must express my gratitude to

from the International Student Office, Congressman

for their help and support. Thanks are given to

for her excellent work of typing this thesis. I would like to thank my wife for her patience and understanding.

TABLE OF CONTENTS

Page

LIST OF FIGURES

CHAPTER I

INTRODUCTION

1.1 Stages of Transition

Experimental studies on the transition from a laminar two-dimensional boundary layer to a turbulent boundary layer over flat plates using hot wire anemometers [1-12] and flow visualization [13-18] have revealed that transition takes place in several stages. First two-dimensional (2-D) Tollmien-Schlichting (T-S) waves appear and propagate downstream, these waves are selectively amplified by the boundary layer, then the higher harmonics of the (T-S) waves are generated, and the mean flow is distorted. In the next stage of transition a spanwise variation in the disturbance field starts to show up, this variation increases and eventually sets in strong three-dimensionality in both the disturbance field and the mean flow. This stage is followed by the development of inflectional instantaneous velocity profiles with embedded high-shear layers at the peak positions. Following this, two types of transition can take place. In the first type, small-scale high frequency oscillations (spikes) are formed in the neighborhood of the shear layers thus setting in irregular motion and leading to breakdown of the laminar flow. The second type of transition is characterized by a low-frequency breakdown of a laminar flow (without formation of turbulent spots) through excitation of a subharmonic wave and incommensurable low frequency fluctuations and by the filling of the spectrum as a result of a nonlinear interaction of high- and low-frequency disturbances.

1.2 Experimental View of Three-Dimensional Phenomena

The spontaneous spanwise variation of the amplitude of the disturbance and the onset of three-dimensionality was observed to appear before the breakdown of the boundary layer. Schubauer and Skramstad [19] and Klebanoff and Tidstrom [1] observed strong three-dimensional effects preceding the birth of turbulent spots. Hama, Long and Hegarty [13], Fales [20] and Weske [21] using a dye technique in water have demonstrated the occurrence of characteristic three-dimensional configurations before transition occurs. Klebanoff, Tidstrom and Sargent [2] performed an experiment which primarily aimed at disclosing the nature of motions in the nonlinear range of boundary-layer instability and the onset of turbulence. They observed that the study of the three-dimensional effects, which was described by Schubauer and Skramstad [19] and Klebanoff and Tidstrom [1] was complicated by small pre-existing spanwise mean-flow variations because they obscure the development of a three-dimensional wave. Hence, they removed these irregularities through the installment of new damping screens in the wind tunnel and a uniform mean flow with hardly detectable variations was observed. Nevertheless, they continued to observe the development of a three-dimensionality characterized by spanwise variations in wave amplitude, indicating that the development of the three-dimensionality is an important aspect of boundary-layer instability. Consequently, in order to study the structure and significance of the observed three-dimensionality, they controlled the spanwise variation in wave amplitude

by placing strips of cellophane tape on the surface beneath the vibrating ribbon.

Figure 1 (Fig. 11 of Klebanoff, Tidstrom and Sargent [2]) shows the spanwise distributions of W/U_1, U/U_1, w'/U_1, and u'/U_1, where W, U, w' and u' are, respectively, the spanwise component of the mean velocity, the streamwise component of the mean velocity, the spanwise fluctuating component of the velocity, and the streamwise fluctuating component of the velocity. Here U_1 is the free-streamwise velocity. Figure 1 demonstrates that the wave amplitude exhibits an almost periodic variation in the spanwise direction about a nonzero mean and an associated spanwise variation in the mean flow whose maxima and minima occur at the peaks and valleys of the fluctuations. The result is a spanwise alternating peak and valley structure (Λ-shaped vortex loops), known as peak-valley splitting. This indicates the generation of longitudinal or streamwise vortices. The Λ- or horseshoe-structure was earlier observed to form and develop in the flow visualization experiments.

The experiments of Klebanoff et al. [2] showed the spontaneous growth of oblique waves having a frequency that is near that of the primary T-S wave, but they did not provide any evidence of the generation of subharmnoic oblique waves. Kachanov, Kozlov and Levchenko [8] were the first to provide an evidence for the excitation of subharmonic waves. In their experiment they specified a fairly large amplitude of the wave, from the very onset, and studied mainly the spectral composition of the disturbance field. They noted from the

spectrum of the disturbance that after the appearance of the fundamental wave and its harmonics there comes a region which is characterized by the appearance and growth of certain low-frequency disturbances which should be attenuated according to the linear theory. At the end of this region the entire low-frequency part of the spectrum begins to grow with a distinguishable harmonic with a frequency equal to one-half the frequency of the fundamental wave which is called subharmonic. The excitation of the subharmonic was considered afterwards in the experiments of Kachanov and Levchenko [9], Saric and Thomas [17] and Corke and Mangano [22]. Saric and Thomas [17] demonstrated the excitation of the subharmonic using flow visualization with smoke-wire streaklines and hot wire anemometer data. They noted the occurrence of the staggered Λ-shaped vortices (Fig. 2.a) at low amplitudes of the fundamental wave. These vortices repeat every $2\lambda_x$ where λ_x is the wave length of the T-S wave, thus indicating a subharmonic of the T-S wave. At high T-S wave amplitudes they observed the occurrence of peak-valley splitting (Fig. 2.b) in which the peaks and valleys are aligned and repeat every λ_x.

Kachanov and Levchenko [9] studied experimentally the three-dimensional resonant interaction of a plane T-S wave having a frequency f_1 with a pair of oblique waves having frequencies $\frac{1}{2} f_1$. They carried out their experiment at not too large values of initial amplitudes of disturbances. They noticed the interaction to be a parametric resonance, resulting in the amplification of small random priming

(background) oscillations of frequency $\frac{1}{2} f_1$ and of a packet of low-frequency oscillations.

Figure 3 (Fig. 23a of Kachanov and Levchenko [9]) shows the streamwise variation of the amplitude of the 2-D T-S wave, the subharmonic wave and other higher-order generated frequencies when (F = 111.4 Hz, F = 124 $x10^{-6}$). This figure shows clearly the fast growth of the subharmonic compared with the growth of the T-S wave.

Figure 4 (Fig. 22 of Kachanov and Levchenko [9]) shows the variation of the phase of the T-S wave and the subharmonic across the boundary-layer, as well as the variation of the root mean square value of the disturbance amplitude for both the T-S and the subharmonic waves. Measurements are based on the streamwise component and are done at F = 124 x 10^{-6} and R = 608 which approximately corresponds to branch two of the neutral stability curve.

Corke and Mangano [22] used the simultaneous generation of phase-coupled plane T-S waves and oblique waves with respective wavenumbers $(\alpha_1,0)$ and (α_2,β_1), (α_2,β_2) to study the growth of three-dimensional disturbances. To accomplish this they used a computer controlled array of line heaters to produce spanwise-moving periodic velocity inflections.

1.3 Review of Analytical Modeling of the Subharmonic Instability

Mainly there are two analytical models to study the subharmonic instability in boundary layers, these are the resonant triad model and the parametric instability model.

1.3.1 Resonant Triads

Raetz [23,24] and Stuart [25] established the occurrence of triad resonances for certain waves which are neutrally stable according to the linear theory, and Lekoudis [26] established the occurrence of triad resonances over a swept wing. Lekoudis [26] found that in the case of a three-dimensional boundary layer and within the considered parameters all three waves are linearly unstable which could make the interaction much stronger than in the case of a Blasius boundary layer. Craik [27-29] established the occurrence of triad resonances over a flat plate. Specifically he found that a two-dimensional wave

$$u = a\, \zeta_1(y)\, e^{2i(\alpha x-\omega t)} + cc$$

forms a resonant triad with the two three-dimensional waves

$$u_1 = a_1\xi_1(y)e^{i(\alpha x-\beta z-\omega t)} + cc$$

and

$$u_2 = a_2\xi_2(y)e^{i(\alpha x+\beta z-\omega t)} + cc$$

Then using temporal instability analysis he derived the equations governing the modulation of the amplitudes a, a_1 and a_2 with time. He found that the amplitudes become indefinitely large at a finite time, an explosive instability. Usher and Craik [38,39] extended the temporal instability of resonant triads to third order and examined the instability of shear flows. Lekoudis [30] derived the equations governing the modulation in space and time of the amplitudes of the waves forming the resonant triad by relaxing the assumption of perfect

resonance. Volodin and Zelman [49] computed the interaction coefficients and presented some results.

1.3.2 Parametric Instability

In the parametric instability model the basic flow is viewed as a combination of the Blasius profile and the two-dimensional T-S wave which makes the basic flow almost streamwise periodic and one method of solution is to apply Floquet theory to derive the equations governing the subharmonic mode along with the boundary conditions. This will yield an eigenvalue problem which is solved locally to compute the rate of growth and the eigenfunction of the subharmonic mode.

Kelly [31] used Floquet theory to study the stability of an inviscid free-shear layer and Maseev [32] was the first to apply Floquet theory to boundary-layer instability. Nayfeh and Bozatli [37] analyzed the stability of a two-dimensional secondary T-S wave whose wavenumber and frequency are nearly one-half those of a fundamental two-dimensional T-S wave. They found that the fundamental wave acts as a parametric exciter for the secondary wave provided that the amplitude of the fundamental wave exceeds a critical value which is proportional to the detuning of the two waves. Herbert [33-35] applied Floquet theory to formulate the subharmonic instability problem. He solved the problem using collocation method with Chebyshev polynomials, his results are in good agreement with the experimental data of Kachanov and Levchenko [9]. Herbert [33] traced the eigenvalues of the subharmonic instability problem for amplitudes of the two-dimensional wave decreasing to $A = 0$.

He found that at a spanwise wavenumber at which the three-dimensional Orr-Sommerfeld mode is almost tuned with a two-dimensional T-S wave, a direct link exists to the subharmonic Orr-Sommerfeld modes in Craik's triad, whereas at a spanwise wavenumber close to that noted in the experiment [9], the dominant subharmonic mode is directly linked to the Squire modes. Herbert [33] concluded that the triad resonance with Squire modes is considered the cause for the broad band of spanwise wavenumbers that may lead to instability.

CHAPTER II

RESONANT TRIAD FORMULATION

To construct a theoretical model of the transition process, we consider a three-dimensional, incompressible, unsteady flow over a flat plate, neglecting body forces. Such a flow is governed by the dimensional Navier-Stokes equations

$$\frac{\partial u^*}{\partial x^*} + \frac{\partial v^*}{\partial y^*} + \frac{\partial w^*}{\partial z^*} = 0 \tag{2.1}$$

$$\frac{\partial u^*}{\partial t^*} + u^* \frac{\partial u^*}{\partial x^*} + v^* \frac{\partial u^*}{\partial y^*} + w^* \frac{\partial u^*}{\partial z^*} + \frac{1}{\rho^*} \frac{\partial p^*}{\partial x^*} - \nu^* \nabla^{*2} u^* = 0 \tag{2.2}$$

$$\frac{\partial v^*}{\partial t^*} + u^* \frac{\partial v^*}{\partial x^*} + v^* \frac{\partial v^*}{\partial y^*} + w^* \frac{\partial v^*}{\partial z^*} + \frac{1}{\rho^*} \frac{\partial p^*}{\partial y^*} - \nu^* \nabla^{*2} v^* = 0 \tag{2.3}$$

$$\frac{\partial w^*}{\partial t^*} + u^* \frac{\partial w^*}{\partial x^*} + v^* \frac{\partial w^*}{\partial y^*} + w^* \frac{\partial w^*}{\partial z^*} + \frac{1}{\rho^*} \frac{\partial p^*}{\partial z^*} - \nu^* \nabla^{*2} w^* = 0 \tag{2.4}$$

where

$$\nabla^{*2} = \frac{\partial^2}{\partial x^{*2}} + \frac{\partial^2}{\partial y^{*2}} + \frac{\partial^2}{\partial z^{*2}}$$

Equation (2.1) is the continuity equation and Equations (2.2)-(2.4) are the x*, y* and z* components of the momentum equation, respectively. Here, u*, v* and w* are the velocity components in the x*, y* and z* directions, p* is the pressure, x* is the streamwise coordinate, y* is the coordinate normal to the plate, and z* is in the plane of the plate such that x*, y* and z* form a right-handed orthogonal system, ρ^* is the fluid density, ν^* is the kinematic viscosity μ^*/ρ^*, μ^* is the viscosity coefficient, and U_∞^* is the freestream velocity.

2.1 The Mean Flow

The mean flow is taken to be two dimensional and steady. For such a flow, Equations (2.1)-(2.4) reduce to

$$\frac{\partial u^*}{\partial x^*} + \frac{\partial v^*}{\partial y^*} = 0 \tag{2.5}$$

$$u^* \frac{\partial u^*}{\partial x^*} + v^* \frac{\partial u^*}{\partial y^*} + \frac{1}{\rho^*} \frac{\partial p^*}{\partial x^*} - \nu^* \nabla^{*2} u^* = 0 \tag{2.6}$$

$$u^* \frac{\partial v^*}{\partial x^*} + v^* \frac{\partial v^*}{\partial y^*} + \frac{1}{\rho^*} \frac{\partial p^*}{\partial y^*} - \nu^* \nabla^{*2} v^* = 0 \tag{2.7}$$

where

$$\nabla^{*2} = \frac{\partial^2}{\partial x^{*2}} + \frac{\partial^2}{\partial y^{*2}}$$

We introduce the non-dimensional quantities

$$(\tilde{x},\tilde{y}) = \frac{1}{L^*} (x^*,y^*) \tag{2.8}$$

$$(\hat{u},\hat{v}) = \frac{1}{U_\infty^*} (u^*,v^*) \tag{2.9}$$

$$\hat{p} = \frac{1}{\rho^* U_\infty^{*2}} p^* \tag{2.10}$$

where L^* is the distance from the leading edge of the plate to a reference point. Substituting Equations (2.8)-(2.10) into Equations (2.5)-(2.7), we obtain

$$\frac{\partial \hat{u}}{\partial \tilde{x}} + \frac{\partial \hat{v}}{\partial \tilde{y}} = 0 \tag{2.11}$$

$$\hat{u} \frac{\partial \hat{u}}{\partial \tilde{x}} + \hat{v} \frac{\partial \hat{u}}{\partial \tilde{y}} + \frac{\partial \hat{p}}{\partial \tilde{x}} - \frac{1}{Re} \tilde{\nabla}^2 \hat{u} = 0 \tag{2.12}$$

$$\hat{u} \frac{\partial \hat{v}}{\partial \tilde{x}} + \hat{v} \frac{\partial \hat{v}}{\partial \tilde{y}} + \frac{\partial \hat{p}}{\partial \tilde{y}} - \frac{1}{Re} \tilde{\nabla}^2 \hat{v} = 0 \tag{2.13}$$

where

$$\tilde{\nabla}^2 = \frac{\partial^2}{\partial \tilde{x}^2} + \frac{\partial^2}{\partial \tilde{y}^2}$$

and

$$Re = U^*_\infty L^*/\nu^* \tag{2.14}$$

An asymptotic solution of Equations (2.11)-(2.13) in the limit of $Re \to \infty$ is given by the Blasius solution

$$U \approx f'(\eta) \tag{2.15}$$

$$V \approx \frac{1}{2\sqrt{\tilde{x}Re}} [\eta f'(\eta) - f(\eta)] \tag{2.16}$$

$$P \approx \text{constant} \tag{2.17}$$

where

$$\eta = \tilde{y}\sqrt{Re}/\sqrt{\tilde{x}} \tag{2.18}$$

and f is governed by the problem

$$f''' + \frac{1}{2} f f'' = 0 \tag{2.19}$$

$$f = f' = 0 \quad \text{at} \quad \eta = 0 \tag{2.20}$$

$$f' \to 1 \quad \text{as} \quad \eta \to \infty \tag{2.21}$$

2.2 The Stability Problem

To formulate the stability problem we start by scaling the variables in Equations (2.1)-(2.4). Thus, we introduce the following non-dimensional quantities:

$$(x,y,z) = \frac{1}{\delta^*_r} (x^*,y^*,z^*) \tag{2.22}$$

$$t = \frac{U^*_\infty}{\delta^*_r} t^* \tag{2.23}$$

$$(\hat{u},\hat{v},\hat{w}) = \frac{1}{U^*_\infty} (u^*,v^*,w^*) \tag{2.24}$$

$$\hat{p} = \frac{1}{\rho^* U^{*2}_\infty} p^* \tag{2.25}$$

where δ_r^* is a dimensional length scale to be specified later. Substituting Equations (2.22)-(2.25) into Equations (2.1)-(2.4), we obtain

$$\frac{\partial \hat{u}}{\partial x} + \frac{\partial \hat{v}}{\partial y} + \frac{\partial \hat{w}}{\partial z} = 0 \tag{2.26}$$

$$\frac{\partial \hat{u}}{\partial t} + \hat{u}\frac{\partial \hat{u}}{\partial x} + \hat{v}\frac{\partial \hat{u}}{\partial y} + \hat{w}\frac{\partial \hat{u}}{\partial z} + \frac{\partial \hat{p}}{\partial x} - \frac{1}{R}\nabla^2\hat{u} = 0 \tag{2.27}$$

$$\frac{\partial \hat{v}}{\partial t} + \hat{u}\frac{\partial \hat{v}}{\partial x} + \hat{v}\frac{\partial \hat{v}}{\partial y} + \hat{w}\frac{\partial \hat{v}}{\partial z} + \frac{\partial \hat{p}}{\partial y} - \frac{1}{R}\nabla^2\hat{v} = 0 \tag{2.28}$$

$$\frac{\partial \hat{w}}{\partial t} + \hat{u}\frac{\partial \hat{w}}{\partial x} + \hat{v}\frac{\partial \hat{w}}{\partial y} + \hat{w}\frac{\partial \hat{w}}{\partial z} + \frac{\partial \hat{p}}{\partial z} - \frac{1}{R}\nabla^2\hat{w} = 0 \tag{2.29}$$

where

$$\nabla^2 = \frac{\partial^2}{\partial x^2} + \frac{\partial^2}{\partial y^2} + \frac{\partial^2}{\partial z^2}$$

and

$$R = U_\infty^* \delta_r^* / \nu^* \tag{2.30}$$

To study the stability of a certain mean flow, we start by solving the problem governing that mean flow. Then we superimpose on that mean flow a disturbance to obtain the total flow

$$\hat{u} = U + u \tag{2.31}$$

$$\hat{v} = V + v \tag{2.32}$$

$$\hat{w} = 0 + w \tag{2.33}$$

$$\hat{p} = P + p \tag{2.34}$$

Substituting Equations (2.31)-(2.34) into Equations (2.26)-(2.29) and subtracting the mean-flow quantities, we obtain

$$\frac{\partial u}{\partial x} + \frac{\partial v}{\partial y} + \frac{\partial w}{\partial z} = 0 \tag{2.35}$$

$$\frac{\partial u}{\partial t} + U\frac{\partial u}{\partial x} + v\frac{\partial U}{\partial y} + \frac{\partial p}{\partial x} - \frac{1}{R}\nabla^2 u + \left[u\frac{\partial U}{\partial x} + V\frac{\partial u}{\partial y}\right] + \left\{u\frac{\partial u}{\partial x} + v\frac{\partial u}{\partial y} + w\frac{\partial u}{\partial z}\right\} = 0 \tag{2.36}$$

$$\frac{\partial v}{\partial t} + U\frac{\partial v}{\partial x} + \frac{\partial p}{\partial y} - \frac{1}{R}\nabla^2 v + \left[u\frac{\partial V}{\partial x} + V\frac{\partial v}{\partial y} + v\frac{\partial V}{\partial y}\right] + \left\{u\frac{\partial v}{\partial x} + v\frac{\partial v}{\partial y} + w\frac{\partial v}{\partial z}\right\} = 0 \tag{2.37}$$

$$\frac{\partial w}{\partial t} + U\frac{\partial w}{\partial x} + \frac{\partial p}{\partial z} - \frac{1}{R}\nabla^2 w + \left[V\frac{\partial w}{\partial y}\right] + \left\{u\frac{\partial w}{\partial x} + v\frac{\partial w}{\partial y} + w\frac{\partial w}{\partial z}\right\} = 0 \tag{2.38}$$

The terms in the square brackets are due to the growth of the boundary layer (nonparallel terms) and the terms in the curly brackets are due to the nonlinearity.

2.3 The Quasi-Parallel Assumption

Linearizing Equations (2.35)-(2.38), we have

$$\frac{\partial u}{\partial x} + \frac{\partial v}{\partial y} + \frac{\partial w}{\partial z} = 0 \tag{2.39}$$

$$\frac{\partial u}{\partial t} + U\frac{\partial u}{\partial x} + v\frac{\partial U}{\partial y} + \frac{\partial p}{\partial x} - \frac{1}{R}\nabla^2 u + \left[u\frac{\partial U}{\partial x} + V\frac{\partial u}{\partial y}\right] = 0 \tag{2.40}$$

$$\frac{\partial v}{\partial t} + U\frac{\partial v}{\partial x} + \frac{\partial p}{\partial y} - \frac{1}{R}\nabla^2 v + \left[u\frac{\partial V}{\partial x} + V\frac{\partial v}{\partial y} + v\frac{\partial V}{\partial y}\right] = 0 \tag{2.41}$$

$$\frac{\partial w}{\partial t} + U\frac{\partial w}{\partial x} + \frac{\partial p}{\partial z} - \frac{1}{R}\nabla^2 w + \left[V\frac{\partial w}{\partial y}\right] = 0 \tag{2.42}$$

If the mean flow is a truly parallel flow, of which an example is a channel flow, then V is zero and U is a function of y only. For such a flow the terms in the square brackets (the nonparallel terms) in

Equations (2.39)-(2.42) are equal to zero and Equations (2.39)-(2.42) reduce to

$$\frac{\partial u}{\partial x} + \frac{\partial v}{\partial y} + \frac{\partial w}{\partial z} = 0 \tag{2.43}$$

$$\frac{\partial u}{\partial t} + U\frac{\partial u}{\partial x} + v\frac{dU}{dy} + \frac{\partial p}{\partial x} - \frac{1}{R}\nabla^2 u = 0 \tag{2.44}$$

$$\frac{\partial v}{\partial t} + U\frac{\partial v}{\partial x} + \frac{\partial p}{\partial y} - \frac{1}{R}\nabla^2 v = 0 \tag{2.45}$$

$$\frac{\partial w}{\partial t} + U\frac{\partial w}{\partial x} + \frac{\partial p}{\partial z} - \frac{1}{R}\nabla^2 w = 0 \tag{2.46}$$

Equations (2.43)-(2.46) are in separable form and permit the normal-mode solution

$$(u,v,p,w) = \{\underline{u}(y),\underline{v}(y),\underline{p}(y),\underline{w}(y)\}\, e^{i(\underline{\alpha}x+\underline{\beta}z-\underline{\omega}t)} + cc \tag{2.47}$$

In the present study, however, we are considering the stability of a two-dimensional boundary-layer flow over a flat plate. Such a flow has a boundary layer which grows in the streamwise direction, and if we view the disturbance as a constant frequency wave propagating in that direction then the wavenumber and the mode shape of such a wave are functions of the streamwise direction due to the nonuniformity of the medium. This means that due to the growth of the boundary layer, the nonparallel terms in Equations (2.39)-(2.42) are nonzero. Consequently, they are not separable and the normal mode form (2.47) is not a solution. However, if we assume that the boundary-layer growth is small over a wavelength, then the wave motion is determined by the local boundary-layer profile and the nonparallel terms can be neglected. This assumption is called the quasi-parallel or lcoally-parallel assumption.

With the quasi-parallel assumption in mind, we choose the length scale δ_r^* to be

$$\delta_r^* = \sqrt{\nu^* x^* / U_\infty^*} \tag{2.48}$$

We note from the definition of δ_r^* in Equation (2.48) that it is proportional to the boundary-layer thickness. Furthermore, using Equation (2.48) in Equation (2.30) yields

$$R = \sqrt{U_\infty^* x^* / \nu^*} \tag{2.49}$$

or

$$R = \sqrt{Re_x} \tag{2.50}$$

where

$$Re_x = U_\infty^* x^* / \nu^* \tag{2.51}$$

In the non-parallel theories [41-46], either the method of multiple scales or the method of averaging is used. Both methods are equivalent and in both methods the non-parallel terms in Equations (2.39)-(2.42) are retained. In the method of averaging, the mean flow quantities are assumed to be slowly varying with the streamwise direction and thus they are written as

$$U = U(x,y) \tag{2.52}$$

$$V = V(x,y) \tag{2.53}$$

with V being small compared with U. Furthermore, the disturbances are assumed to have the following more general normal-mode form

$$(u,v,p,w) = A(x)\{\underline{u}(x,y),\underline{v}(x,y),\underline{p}(x,y),\underline{w}(x,y)\}e^{i\theta} \tag{2.54}$$

where

$$\theta = \int \alpha dx + \beta z - \omega t \tag{2.55}$$

and A(x) is the complex amplitude function. In the form given by Equations (2.54) and (2.55), A, $\underline{u}$, $\underline{v}$, $\underline{p}$, $\underline{w}$ and α are all assumed to be slowly varying functions of x. Substituting Equations (2.52)-(2.55) into Equations (2.39)-(2.42) and placing the small terms on the right-hand side as an inhomogeneity, the left-hand side is then recognized as the quasi-parallel problem. Then a solvability condition is derived which expresses the modulation of the complex amplitude A(x) in the streamwise direction. So, even in the non-parallel theories, the stability problem that we solve is quasi-parallel.

2.4 The 3-D Disturbance Linear Quasi-Parallel Problem

We consider the linear quasi-parallel problem. Then Equations (2.35)-(2.38) reduce to

$$\frac{\partial u}{\partial x} + \frac{\partial v}{\partial y} + \frac{\partial w}{\partial z} = 0 \tag{2.56}$$

$$\frac{\partial u}{\partial t} + U \frac{\partial u}{\partial x} + v \frac{\partial U}{\partial y} + \frac{\partial p}{\partial x} - \frac{1}{R} \nabla^2 u = 0 \tag{2.57}$$

$$\frac{\partial v}{\partial t} + U \frac{\partial v}{\partial x} + \frac{\partial p}{\partial y} - \frac{1}{R} \nabla^2 v = 0 \tag{2.58}$$

$$\frac{\partial w}{\partial t} + U \frac{\partial w}{\partial x} + \frac{\partial p}{\partial z} - \frac{1}{R} \nabla^2 w = 0 \tag{2.59}$$

The boundary conditions consist of the no-slip and no-penetration conditions at the wall

$$u = v = w = 0 \quad \text{at} \quad y = 0 \tag{2.60}$$

and the vanishing of all disturbances away from the wall

$$u,v,w,p \to 0 \quad \text{as} \quad y \to \infty \tag{2.61}$$

We seek a solution of Equations (2.56)-(2.61) in the normal form

$$u = \cos\beta z[\xi_1(y)e^{i\theta_1} + cc] \tag{2.62}$$

$$v = \cos\beta z[\xi_3(y)e^{i\theta_1} + cc] \tag{2.63}$$

$$p = \cos\beta z[\xi_4(y)e^{i\theta_1} + cc] \tag{2.64}$$

$$w = \sin\beta z[\xi_5(y)e^{i\theta_1} + cc] \tag{2.65}$$

where

$$\theta_1 = \int \alpha_1 dx - \omega_1 t \tag{2.66}$$

and cc stands for the complex conjugate of the preceding terms. In Equations (2.62)-(2.66), β is the spanwise wavenumber (β is real), α_1 is the streamwise wavenumber, and ω_1 is the frequency. In spatial stability analyses, ω_1 is real and α_1 is complex with $-\alpha_{1i}$ being the spatial rate of growth, where α_{1i} is the imaginary part of α_1. In temporal stability analyses, α_1 is real and ω_1 is complex with ω_{1i} being the temporal rate of growth, where ω_{1i} is the imaginary part of ω_1.

Substituting Equations (2.62)-(2.65) into Equations (2.56)-(2.61) yields the eigenvalue problem

$$i\alpha_1\xi_1 + D\xi_3 + \beta\xi_5 = 0 \tag{2.67}$$

$$-\frac{1}{R}D^2\xi_1 + \frac{\Lambda}{R}\xi_1 + DU\xi_3 + i\alpha_1\xi_4 = 0 \tag{2.68}$$

$$-\frac{1}{R}D^2\xi_3 + \frac{\Lambda}{R}\xi_3 + D\xi_4 = 0 \tag{2.69}$$

$$-\frac{1}{R}D^2\xi_5 + \frac{\Lambda}{R}\xi_5 - \beta\xi_4 = 0 \tag{2.70}$$

$$\xi_1 = \xi_3 = \xi_5 = 0 \quad \text{at} \quad y = 0 \tag{2.71}$$

$$\xi_n \to 0 \quad \text{as} \quad y \to \infty \tag{2.72}$$

where

$$\Lambda = \alpha_1^2 + \beta^2 + iR(\alpha_1 U - \omega_1) \tag{2.73}$$

and

$$D = \frac{\partial}{\partial y} .$$

2.5 The Adjoint Problem of the 3-D Linear Quasi-Parallel Problem

In Section 2.9 the adjoint is used to derive the solvability condition for the resonant triad. In this section we define the adjoint problem of the 3-D linear quasi-parallel problem defined by Equations (2.67)-(2.73). To accomplish this, we multiply Equation (2.67) by ξ_4^*, Equation (2.68) by ξ_1^*, Equation (2.69) by ξ_3^*, and Equation (2.70) by ξ_5^*, add the resulting equations, integrate the result by parts from y = 0 to y = ∞, and obtain

$$\begin{aligned}
&\xi_4^*\xi_3\Big|_0^\infty - \int_0^\infty \xi_3 D\xi_4^* dy + \int_0^\infty (i\alpha_1\xi_1 + \beta\xi_5)\xi_4^* dy \\
&+ \int_0^\infty \left(\frac{\Lambda}{R}\xi_1 + DU\xi_3 + i\alpha_1\xi_4\right)\xi_1^* dy - \frac{\xi_1^* D\xi_1 - \xi_1 D\xi_1^*}{R}\Big|_0^\infty \\
&- \int_0^\infty \frac{\xi_1 D^2\xi_1^*}{R}\, dy + \int_0^\infty \frac{\Lambda}{R}\xi_3\xi_3^* dy + \xi_3^*\xi_4\Big|_0^\infty \\
&- \int_0^\infty \xi_4 D\xi_3^* - \frac{\xi_3^* D\xi_3 - \xi_3 D\xi_3^*}{R}\Big|_0^\infty - \int_0^\infty \frac{\xi_3 D^2\xi_3^*}{R}\, dy \\
&+ \int_0^\infty \left(\frac{\Lambda}{R}\xi_5 - \beta\xi_4\right)\xi_5^* dy - \frac{\xi_5^* D\xi_5 - \xi_5 D\xi_5^*}{R}\Big|_0^\infty - \int_0^\infty \frac{\xi_5 D^2\xi_5^*}{R}\, dy = 0
\end{aligned} \tag{2.74}$$

Collecting the coefficients of ξ_1, ξ_3, ξ_4 and ξ_5, we rewrite (2.74) as

$$\left[\xi_4^*\xi_3 - \frac{\xi_1^*D\xi_1 - \xi_1 D\xi_1^*}{R} + \xi_3^*\hat{\xi}_4 - \frac{\xi_3^*D\xi_3 - \xi_3 D\xi_3^*}{R}\right.$$

$$\left. - \frac{\xi_5^*D\xi_5 - \xi_5 D\xi_5^*}{R}\right]_0^\infty + \int_0^\infty \left[\xi_4\{i\alpha_1\xi_1^* - D\xi_3^* - \beta\xi_5^*\}\right.$$

$$+ \xi_1\{i\alpha_1\xi_4^* + \frac{\Lambda}{R}\xi_1^* - \frac{1}{R}D^2\xi_1^*\} + \xi_3\{-D\xi_4^* + DU\xi_1^* + \frac{\Lambda}{R}\xi_3^* - \frac{1}{R}D^2\xi_3^*\}$$

$$\left. + \xi_5\{\beta\xi_4^* + \frac{\Lambda}{R}\xi_5^* - \frac{1}{R}D^2\xi_5^*\}\right]dy = 0 \qquad (2.75)$$

We define the adjoint equations by setting each of the coefficients of ξ_4, ξ_1, ξ_3 and ξ_5 equal to zero; that is

$$i\alpha_1\xi_1^* - D\xi_3^* - \beta\xi_5^* = 0 \qquad (2.76)$$

$$-\frac{1}{R}D^2\xi_1^* + \frac{\Lambda}{R}\xi_1^* + i\alpha_1\xi_4^* = 0 \qquad (2.77)$$

$$-\frac{1}{R}D^2\xi_3^* + \frac{\Lambda}{R}\xi_3^* + DU\xi_1^* - D\xi_4^* = 0 \qquad (2.78)$$

$$-\frac{1}{R}D^2\xi_5^* + \frac{\Lambda}{R}\xi_5^* + \beta\xi_4^* = 0 \qquad (2.79)$$

Then, Equation (2.75) reduces to

$$\left[\xi_4^*\xi_3 - \frac{\xi_1^*D\xi_1 - \xi_1 D\xi_1^*}{R} + \xi_3^*\xi_3 - \frac{\xi_3^*D\xi_3 - \xi_3 D\xi_3^*}{R}\right.$$

$$\left. - \frac{\xi_5^*D\xi_5 - \xi_5 D\xi_5^*}{R}\right]_0^\infty = 0$$

We use Equations (2.71) and (2.72) in the above equation, and then choose the boundary conditions of the adjoint problem to be

$$\xi_1^* = \xi_3^* = \xi_5^* = 0 \quad \text{at} \quad y = 0 \qquad (2.80)$$

and

$$\xi_n^* \to 0 \quad \text{as} \quad y \to \infty \tag{2.81}$$

2.6 The 2-D Disturbance Linear Quasi-Parallel Problem

We consider a two-dimensional disturbance instead of a three-dimensional disturbance, and let

$$u = \zeta_1(y)e^{i\theta} + cc \tag{2.82}$$

$$v = \zeta_3(y)e^{i\theta} + cc \tag{2.83}$$

$$p = \zeta_4(y)e^{i\theta} + cc \tag{2.84}$$

$$w = 0 \tag{2.85}$$

where

$$\theta = \int \alpha dx - \omega t \tag{2.86}$$

Substituting Equations (2.82)-(2.85) into Equations (2.56)-(2.61), we obtain

$$i\alpha\zeta_1 + D\zeta_3 = 0 \tag{2.87}$$

$$-\frac{1}{R}D^2\zeta_1 + \frac{\Gamma}{R}\zeta_1 + DU\zeta_3 + i\alpha\zeta_4 = 0 \tag{2.88}$$

$$-\frac{1}{R}D^2\zeta_3 + \frac{\Gamma}{R}\zeta_3 + D\zeta_4 = 0 \tag{2.89}$$

$$\zeta_1 = \zeta_3 = 0 \quad \text{at} \quad y = 0 \tag{2.90}$$

$$\zeta_n \to 0 \quad \text{as} \quad y \to \infty \tag{2.91}$$

where

$$\Gamma = \alpha^2 + iR(\alpha U - \omega) \tag{2.92}$$

2.7 The Adjoint Problem of the 2-D Linear Quasi-Parallel Problem

The adjoint problem of the two-dimensional linear quasi-parallel problem is governed by the equations

$$i\alpha\zeta_1^* - D\zeta_3^* = 0 \tag{2.93}$$

$$-\frac{1}{R}D^2\zeta_1^* + \frac{\Gamma}{R}\zeta_1^* + i\alpha\zeta_4^* = 0 \tag{2.94}$$

$$-\frac{1}{R}D^2\zeta_3^* + \frac{\Gamma}{R}\zeta_3^* + DU\zeta_1^* - D\zeta_4^* = 0 \tag{2.95}$$

and the boundary conditions

$$\zeta_1^* = \zeta_3^* = 0 \quad \text{at} \quad y = 0 \tag{2.96}$$

$$\zeta_n^* \to 0 \quad \text{as} \quad y \to \infty \tag{2.97}$$

2.8 The Resonant Triad Problem

In the resonant triad model, we consider the mean flow to be a solution (or an approximate solution) of Equations (2.11)-(2.13) and the appropriate boundary conditions and the disturbance as a superposition of a two-dimensional wave and two three-dimensional waves traveling at equal but opposite angles with respect to the downstream direction.

Following Nayfeh [36] we use the method of averaging and consider the combined temporal/spatial stability, including the effect of nonparallelism. We seek a solution of Equations (2.35)-(2.38) and the appropriate boundary conditions in the form

$$u = \{A(x,t)\zeta_1(y,x)e^{i\theta} + 2B(x,t)\cos\beta z\,\xi_1(y,x)e^{i\theta_1}\} + cc \tag{2.98}$$

$$v = \{A(x,t)\zeta_3(y,x)e^{i\theta} + 2B(x,t)\cos\beta z\,\xi_3(y,x)e^{i\theta_1}\} + cc \tag{2.99}$$

$$p = \{A(x,t)\zeta_4(y,x)e^{i\theta} + 2B(x,t)\cos\beta z\xi_4(y,x)e^{i\theta_1}\} + cc \qquad (2.100)$$

$$w = 2B(x,t)\sin\beta z\xi_5(y,x)e^{i\theta_1} + cc \qquad (2.101)$$

where the ζ_n and ξ_n are solutions of the two- and three-dimensional quasi-parallel problem corresponding to

$$\theta = \int \alpha dx - \omega t \quad \text{and} \quad \theta_1 = \int \alpha_1 dx - \omega_1 t \qquad (2.102)$$

We assume that

$$\omega_1 \approx \frac{1}{2}\omega \quad \text{and} \quad \alpha_1 \approx \frac{1}{2}\alpha \qquad (2.103)$$

Substituting Equations (2.98)-(2.101) into Equations (2.35)-(2.38) and separating harmonics we obtain

$$e_1 = -\xi_1 \frac{\partial B}{\partial x} - \frac{\partial \xi_1}{\partial x} B \qquad (2.104)$$

$$e_2 = -(U\xi_1 + \xi_4)\frac{\partial B}{\partial x}$$
$$- \xi_1 \frac{\partial B}{\partial t} - [i(\alpha - \bar{\alpha}_1)\zeta_1\bar{\xi}_1 + \zeta_3 D\bar{\xi}_1 + \bar{\xi}_3 D\zeta_1]ABe^{-i(\theta-\theta_1-\bar{\theta}_1)}$$
$$- \left[U\frac{\partial \xi_1}{\partial x} + \frac{\partial \xi_4}{\partial x} + \xi_1\frac{\partial U}{\partial x} + VD\xi_1\right]B \qquad (2.105)$$

$$e_3 = -U\xi_3\frac{\partial B}{\partial x} - \xi_3\frac{\partial B}{\partial t}$$
$$- [i(\alpha\zeta_3\bar{\xi}_1 - \bar{\alpha}_1\zeta_1\bar{\xi}_3) + \zeta_3 D\bar{\xi}_3 + \bar{\xi}_3 D\zeta_3]ABe^{-i(\theta-\theta_1-\bar{\theta}_1)}$$
$$- \left[U\frac{\partial \xi_3}{\partial x} + VD\xi_3 + \xi_3 DV\right]B \qquad (2.106)$$

$$e_4 = -U\xi_5\frac{\partial B}{\partial x} - \xi_5\frac{\partial B}{\partial t}$$
$$- [-i\bar{\alpha}_1\zeta_1\bar{\xi}_5 + \zeta_3 D\bar{\xi}_5]ABe^{-i(\theta-\theta_1-\bar{\theta}_1)}$$
$$- \left[U\frac{\partial \xi_5}{\partial x} + VD\xi_5\right]B \qquad (2.107)$$

$$e_5 = - \zeta_1 \frac{\partial A}{\partial x} - \frac{\partial \zeta_1}{\partial x} A \tag{2.108}$$

$$e_6 = - (U\zeta_1 + \zeta_4) \frac{\partial A}{\partial x}$$

$$- \zeta_1 \frac{\partial A}{\partial t} - 2[i\alpha_1 \xi_1^2 + \xi_3 D\xi_1 - \beta \xi_1 \xi_5] B^2 e^{i(2\theta_1 - \theta)}$$

$$- [U \frac{\partial \zeta_1}{\partial x} + \frac{\partial \zeta_4}{\partial x} + \zeta_1 \frac{\partial U}{\partial x} + VD\zeta_1] A \tag{2.109}$$

$$e_7 = - U\zeta_3 \frac{\partial A}{\partial x} - \zeta_3 \frac{\partial A}{\partial t}$$

$$- 2[i\alpha_1 \xi_1 \xi_3 + \xi_3 D\xi_3 - \beta \xi_3 \xi_5] B^2 e^{i(2\theta_1 - \theta)}$$

$$- [U \frac{\partial \zeta_3}{\partial x} + VD\zeta_3 + \zeta_3 DV] A \tag{2.110}$$

where Λ and Γ are defined in Equations (2.73) and (2.92), respectively, and the bar on top of a certain quantity means the complex conjugate of that quantity.

2.9 Modulation Equations

To derive the equations governing the modulation of the amplitudes B and A with time and space we demand that the residuals e_1, e_2, e_3, and e_4 be orthogonal to the adjoint functions ξ_4^*, ξ_1^*, ξ_3^*, and ξ_5^*. The result is

$$H_1 \frac{\partial B}{\partial t} + H_2 \frac{\partial B}{\partial x} + H_4 B + \Lambda_2 A \bar{B} e^{i(\theta - \theta_1 - \bar{\theta}_1)} = 0 \tag{2.111}$$

where H_1, H_2, H_4 and Λ_2 are defined in Appendix A. Similarly, we demand that the residuals e_5, e_6, and e_7 be orthogonal to ζ_4^*, ζ_1^*, and ζ_3^*. The result is

$$h_1 \frac{\partial A}{\partial t} + h_2 \frac{\partial A}{\partial x} + h_4 A + \Lambda_1 B^2 e^{i(2\theta_1 - \theta)} = 0 \tag{2.112}$$

where h_1, h_2, h_4 and Λ_1 are defined in Appendix A.

We compute the coefficients in Equations (2.111) and (2.112) at different values of R, and then numerically integrate them for certain initial conditions.

CHAPTER III

PARAMETRIC FORMULATION

The resonant triad model is not the only way to model the subharmonic instability problem. In this chapter we consider a second model which utilizes Floquet theory by looking at the problem as a parametric instability problem.

In the Floquet theory model we take the basic flow and the disturbance as quasi-parallel. Furthermore, we assume that the two-dimensional wave affects but is not affected by the three dimensional wave.

In formulating the problem governing the three-dimensional wave, we take the basic flow as a superposition of the Blasius flow and a known two-dimensional disturbance. In Section 3.1 we define the problem, and in Section 3.2 we derive the problem governing the three-dimensional wave.

3.1 Problem Formulation

In the parametric formulation, the basic flow is taken as a superposition of the Blasius flow and a two-dimensional linear quasi-parallel disturbance; that is,

$$U_b = U(y) + A_o[\zeta_1(y)e^{i\theta} + cc] \tag{3.1}$$

$$V_b = A_o[\zeta_3(y)e^{i\theta} + cc] \tag{3.2}$$

where U(y) is the Blasius profile given by Equation (2.15), A_0 is the initial amplitude of the two-dimensional distrubance, θ is given by Equation (2.55), and ζ_n satisfy Equations (2.87)-(2.91). Substituting Equations (3.1) and (3.2) into Equations (2.35)-(2.38), linearizing and neglecting the nonparallel terms, we obtain

$$\frac{\partial u}{\partial x} + \frac{\partial v}{\partial y} + \frac{\partial w}{\partial z} = 0 \tag{3.3}$$

$$\frac{\partial u}{\partial t} + [U + A_0(\zeta_1 e^{i\theta} + cc)]\frac{\partial u}{\partial x} + v[DU + A_0(D\zeta_1 e^{i\theta} + cc)]$$
$$+ A_0(i\alpha\zeta_1 e^{i\theta} + cc)u + A_0(\zeta_3 e^{i\theta} + cc)\frac{\partial u}{\partial y} + \frac{\partial p}{\partial x} - \frac{1}{R}\nabla^2 u = 0 \tag{3.4}$$

$$\frac{\partial v}{\partial t} + [U + A_0(\zeta_1 e^{i\theta} + cc)]\frac{\partial v}{\partial x} + A_0[i\alpha\zeta_3 e^{i\theta} + cc)u$$
$$+ A_0(\zeta_3 e^{i\theta} + cc)\frac{\partial v}{\partial y} + A_0(D\zeta_3 e^{i\theta} + cc)\, v + \frac{\partial p}{\partial y} - \frac{1}{R}\nabla^2 v = 0 \tag{3.5}$$

$$\frac{\partial w}{\partial t} + [U + A_0(\zeta_1 e^{i\theta} + cc)]\frac{\partial w}{\partial x} + A_0(\zeta_3 e^{i\theta} + cc)\frac{\partial w}{\partial y}$$
$$+ \frac{\partial p}{\partial z} - \frac{1}{R}\nabla^2 w = 0 \tag{3.6}$$

3.2 Floquet Approach

Equations (3.3)-(3.6) are linear partial-differential equations whose coefficients are independent of z, periodic in t, and almost periodic in x. If we assume that the coefficients are strictly periodic in x, then it follows from Floquet theory that Equations (3.3)-(3.6) have solutions of the form

$$(u,v,p) = \cos\beta z\, e^{\gamma x+\sigma t} \sum_{n=-\infty}^{\infty} [\psi_{1n}(y), \psi_{3n}(y), \psi_{4n}(y)]e^{\frac{1}{2} in(\alpha_r x-\omega t)} \tag{3.7}$$

$$w = \sin\beta z\, e^{\gamma x+\sigma t} \sum_{n=-\infty}^{\infty} \psi_{5n}(y)e^{\frac{1}{2} in(\alpha_r x-\omega t)} \tag{3.8}$$

For a real solution, we require that

$$\psi_{mn} = \bar{\psi}_{m(-n)} \tag{3.9}$$

The γ and σ are called characteristic exponents and they are complex in general. For temporal stability $\gamma = 0$, whereas for spatial stability $\sigma = 0$. The ψ_{mn} are governed by an infinite system of ordinary differential equations. Since the basic flow with wavenumber α_r provides coupling only between components n and $n \pm 2$, then the system splits into two decoupled systems for even and odd n that correspond to two classes of solutions

$$(u_1, v_1, p_1) = \cos\beta z e^{\gamma x + \sigma t} \sum_{n=-\infty}^{\infty}{}_{n\,even} [\psi_{1n}(y), \psi_{3n}(y), \psi_{4n}(y)] e^{\frac{1}{2} in(\alpha_r x - \omega t)} \tag{3.10}$$

$$w_1 = \sin\beta z\, e^{\gamma x + \sigma t} \sum_{n=-\infty}^{\infty}{}_{n\,even} \psi_{5n}(y) e^{\frac{1}{2} in(\alpha_r x - \omega t)} \tag{3.11}$$

and

$$(u_2, v_2, p_2) = \cos\beta z\, e^{\gamma x + \sigma t} \sum_{n=-\infty}^{\infty}{}_{n\,odd} [\psi_{1n}(y), \psi_{3n}(y), \psi_{4n}(y)] e^{\frac{1}{2} in(\alpha_r x - \omega t)} \tag{3.12}$$

$$w_2 = \sin\beta z\, e^{\gamma x - \sigma t} \sum_{n=-\infty}^{\infty}{}_{n\,odd} \psi_{5n}(y) e^{\frac{1}{2} in(\alpha_r x - \omega t)} \tag{3.13}$$

The solution given by Equations (3.10) and (3.11) is for the fundamental parametric resonance, whereas the solution given by Equations (3.12) and (3.13) is for the subharmonic mode, originating from principal parametric resonance. To solve for the ψ_{mn} and either γ or σ for the subharmonic mode we truncate the series. The lowest possible truncation is to let n take the values 1 and -1, so we let

$$(u, v, p) = \cos\beta z e^{\gamma x + \sigma t} [\{\psi_1(y), \psi_3(y), \psi_4(y)\} e^{\frac{1}{2} i(\alpha_r x - \omega t)} + cc] \tag{3.14}$$

$$w = \sin\beta z\, e^{\gamma x + \sigma t} [\psi_5(y) e^{\frac{1}{2} i(\alpha_r x - \omega t)} + cc] \tag{3.15}$$

The form of the solution given by Equations (3.14) and (3.15), consists of a pair of three-dimensional propagating waves that form a spanwise standing wave. Substituting Equations (3.14) and (3.15) into Equations (3.3)-(3.6), we obtain

$$(\gamma + \tfrac{1}{2} i\alpha_r)\psi_1 + D\psi_3 + \beta\psi_5 = 0 \tag{3.16}$$

$$\begin{aligned}&[(\gamma + \tfrac{1}{2} i\alpha_r)U + \sigma - \tfrac{1}{2} i\omega]\psi_1 + DU\psi_3 + (\gamma + \tfrac{1}{2} i\alpha_r)\psi_4 \\ &\quad - \tfrac{1}{R}[D^2 + (\gamma + \tfrac{1}{2} i\alpha_r)^2 - \beta^2]\psi_1 + A_o e^{-\int \alpha_i dx}[(\gamma + \tfrac{1}{2} i\alpha_r \\ &\quad - \alpha_i)\zeta_1\bar{\psi}_1 + \zeta_3 D\bar{\psi}_1 + D\zeta_1\bar{\psi}_3] = 0\end{aligned} \tag{3.17}$$

$$\begin{aligned}&[(\gamma + \tfrac{1}{2} i\alpha_r)U + \sigma - \tfrac{1}{2} i\omega]\psi_3 + D\psi_4 - \tfrac{1}{R}[D^2 + (\gamma + \tfrac{1}{2} i\alpha_r)^2 - \beta^2]\psi_3 \\ &\quad + A_o e^{-\int \alpha_i dx}[(\gamma - \tfrac{1}{2} i\alpha_r)\zeta_1\bar{\psi}_3 + i\alpha\zeta_3\bar{\psi}_1 + \zeta_3 D\bar{\psi}_3 + \bar{\psi}_3 D\zeta_3] = 0\end{aligned} \tag{3.18}$$

$$\begin{aligned}&[(\gamma + \tfrac{1}{2} i\alpha_r)U + \sigma - \tfrac{1}{2} i\omega]\psi_5 - \beta\psi_4 - \tfrac{1}{R}[D^2 + (\gamma + \tfrac{1}{2} i\alpha_r)^2 - \beta^2]\psi_5 \\ &\quad + A_o e^{-\int \alpha_i dx}[(\gamma - \tfrac{1}{2} i\alpha_r)\zeta_1\bar{\psi}_5 + \zeta_3 D\bar{\psi}_5] = 0\end{aligned} \tag{3.19}$$

The boundary conditions are

$$\psi_1 = \psi_3 = \psi_5 = 0 \quad \text{at} \quad y = 0 \tag{3.20}$$

$$\psi_n \to 0 \quad \text{as} \quad y \to \infty \tag{3.21}$$

CHAPTER IV

METHOD OF SOLUTION

In using the quasi-parallel assumption, which was discussed in Section 2.2, we end up with a stability problem which needs to be solved locally at a constant value of x^* and consequently a constant value of R, due to the definition of R in Equation (2.49). It was also mentioned in Section 2.2, that even in the non-parallel theories, the stability problem that we need to solve is a quasi-parallel problem. This means that the problems derived in Chapters II and III need to be solved locally at a constant value of R and thus R will be treated as a parameter.

4.1. Solution of the Resonant Triad Problem

In Section 2.9 we found the equations governing the modulation of the amplitudes of the two-dimensional wave and the three-dimensional wave to be

$$H_1 \frac{\partial B}{\partial t} + H_2 \frac{\partial B}{\partial x} + H_4 B + \Lambda_2 A B e^{-i(\theta-\theta_1-\bar{\theta}_1)} = 0 \qquad (4.1)$$

$$h_1 \frac{\partial A}{\partial t} + h_2 \frac{\partial A}{\partial x} + h_4 A + \Lambda_1 B^2 e^{i(2\theta_1-\theta)} = 0 \qquad (4.2)$$

where H_1, H_2, H_4, Λ_2, h_1, h_2, h_4 and Λ_1 are defined in Appendix A, θ and θ_1 are defined in Equation (2.102) as

$$\theta = \int \alpha dx - \omega t \quad \text{and} \quad \theta_1 = \int \alpha_1 dx - \omega_1 t \qquad (4.3)$$

Equations (4.1) and (4.2) govern the modulation of the amplitudes A and B with time t and streamwise direction x. However, to solve

Equations (4.1) and (4.2) we consider the spatial and temporal stability problems one at a time.

4.1.1 The Temporal Stability Case

For the case of temporal stability, Equations (4.1) and (4.2) reduce to

$$H_1 \frac{\partial B}{\partial t} + H_4 B + \Lambda_2 A B e^{-i(\theta-\theta_1-\bar{\theta}_1)} = 0 \qquad (4.4)$$

$$h_1 \frac{\partial A}{\partial t} + h_4 A + \Lambda_1 B^2 e^{i(2\theta_1-\theta)} = 0 \qquad (4.5)$$

where θ and θ_1 are given by Equation (4.3) and for this case we have

$$\alpha_1 = \frac{1}{2}\alpha \quad \text{and} \quad \omega_1 \approx \frac{1}{2}\omega \qquad (4.6)$$

α and α_1 are real, whereas ω and ω_1 are complex in general.

To solve Equations (4.4) and (4.5) we need to compute the coefficients H_1, H_4, Λ_2, h_1, h_4 and Λ_1 at some location x. Computing these coefficients will be considered in Section 4.1c. Once the coefficients are known, then for certain initial conditions $A(t_o)$ and $B(t_o)$ we integrate Equations (4.4) and (4.5) in time. This can be done numercially using a Runge-Kutta scheme.

4.1.2 The Spatial Stability Case

For the case of spatial stability, Equations (4.1) and (4.2) reduce to

$$H_2 \frac{\partial B}{\partial x} + H_4 B + \Lambda_2 A B e^{-i(\theta-\theta_1-\bar{\theta}_1)} = 0 \qquad (4.7)$$

$$h_2 \frac{\partial A}{\partial x} + h_4 A + \Lambda_1 B^2 e^{i(2\theta_1-\theta)} = 0 \qquad (4.8)$$

θ and θ_1 are given by Equation (4.3) and for this case we have

$$\alpha_1 \approx \frac{1}{2}\alpha \quad \text{and} \quad \omega_1 = \frac{1}{2}\omega \tag{4.9}$$

where ω and ω_1 are real, whereas α and α_1 are complex in general.

In order to integrate Equtaions (4.7) and (4.8) we need the initial conditions $A(x_0)$ and $B(x_0)$ which we assume. Besides we need to compute the coefficients H_2, H_4, Λ_2, h_2, h_4 and Λ_1 at values of x between the limits of integration x_0 and x_f. Computing the coefficients at some value of x will be considered in Section 4.1.3.

4.1.3 Computing the Coefficients of the Modulation Equations at Some x

In order to compute the coefficients in Equations (4.1) and (4.2) at a certain value of x, we need to know R, α_1, α, ω_1, ω, β, the ξ_n, the ζ_n, the ξ_n^* and the ζ_n^* at that x. So the problem of computing the coefficients at a certain value of x is mainly the problem of solving the problems governing the ξ_n, the ζ_n, the ξ_n^* and the ζ_n^*. Once this is done we have R, α_1, α, ω_1, ω, β, the ξ_n, the ζ_n, the ξ_n^* and the ζ_n^* known and all we need afterwards is to perform the numerical integrations in Appendix A to end up with the required coefficients.

The ξ_n are governed by Equations (2.67)-(2.72), the ζ_n are governed by Equations (2.87)-(2.91), the ξ_n^* are governed by Equations (2.76)-(2.79), (2.80), and (2.81) and the ζ_n^* are governed by Equations (2.93)-(2.97). Since the problems governing the ξ_n, the ζ_n, the ζ_n^* and the ζ_n^* are very much similar in their mathematical nature, we explain the method of solving them by considering the problem governing the ξ_n,

which is the three-dimensional disturbance linear quasi-parallel problem given by Equations (2.67)-(2.72).

4.1.4 Solution of the 3-D Disturbance Linear Quasi-Parallel Problem

The three-dimensional disturbance linear quasi-parallel problem given by Equations (2.67)-(2.72) consists of a system of homogeneous differential equations subject to homogeneous boundary conditions. A nontrivial solution to the problem exists only for a certain combination of α_1, β, ω_1, and R. The eigenvalue problem provides a complex dispersion relation of the form

$$\alpha_1 = \alpha_1(\omega_1, \beta, R) \tag{4.10}$$

The solution to this eigenvalue problem is obtained numerically.

For the temporal stability problem, α_1 and β are real; and values are assigned to α_1, β and R. Then a complex ω_1 can be calculated as an eigenvalue. For the spatial stability problem, we assign real values to ω_1, β and R. Then a complex α_1 can be calculated as an eigenvalue.

To solve the problem given by Equations (2.67)-(2.72) for either the spatial or temporal case, we transform the equations into the system of first-order differential equations

$$D\xi = F\xi \tag{4.11}$$

where

$$\xi = \{\xi_1, \xi_2, \xi_3, \xi_4, \xi_5, \xi_6\}^T \tag{4.12}$$

is a 6x1 vector and F is a 6x6 matrix with elements defined in Appendix B.

Equations (2.71) and (2.72) define respectively the boundary conditions at $y = 0$ and as $y \to \infty$. Since we solve the problem over a finite domain, we need to replace the boundary conditions at infinity with the proper boundary conditions at some finite value of y. We note that for large values of y, say $y \geq y_{max}$, $U \to 1$ and $DU \to 0$, and thus the system of equations given by Equation (4.11) becomes

$$D\xi = F_e \xi \quad \text{for} \quad y \geq y_{max} \tag{4.13}$$

where the matrix F_e is obtained by replacing U and DU in F with 1 and 0, respectively. Since F_e consists of constant elements, the system (4.13) is solved analytically to get

$$\xi = C\hat{\eta} \quad \text{for} \quad y \geq y_{max} \tag{4.14}$$

where

$$\hat{\eta} = \{a_1 e^{\sqrt{\alpha_1^2+\beta^2}\,y}, a_2 e^{\sqrt{\Lambda_e}\,y}, a_3 e^{\sqrt{\Lambda_e}\,y}, a_4 e^{-\sqrt{\alpha_1^2+\beta^2}\,y}, a_5 e^{-\sqrt{\Lambda_e}\,y}, a_6 e^{-\sqrt{\Lambda_e}\,y}\}^T \tag{4.15}$$

$$\Lambda_e = \alpha_1^2 + \beta^2 + iR(\alpha_1 - \omega_1) \tag{4.16}$$

and C is a 6x6 matrix of eigenvectors. It follows from (4.14) that

$$\hat{\eta} = C^{-1}\xi \quad \text{for} \quad y \geq y_{max} \tag{4.17}$$

Due to Equation (2.72), ξ_n must vanish at large y, which means that

$$a_1 = a_2 = a_3 = 0 \quad \text{for} \quad y \geq y_{max} \tag{4.18}$$

and thus our boundary conditions become

$$Q\xi = 0 \quad \text{at} \quad y = y_{max} \tag{4.19}$$

where Q consists of the first three rows of C^{-1}.

The boundary conditions at $y = y_{max}$ given by Equation (4.19), the boundary conditions at $y = 0$ given by Equation (2.71) and the system of differential equations given by Equation (4.11) form a stiff eigenvalue problem. To solve this problem we start with an initial guess of the eigenvalue then we integrate the equations using the computer code called SUPORT developed by Scott and Watts [40]. The code integrates the equations and satisfies as many boundary conditions as possible. If the guessed eigenvalue is not an eigenvalue of the system, the boundary conditions are not fully satisfied and the guessed eigenvalue is updated according to the error at the boundary. A Newton-Raphson scheme is used to iterate on the eigenvalue.

4.2 Solution of the Parametric Instability Problem

To solve the parametric instability problem, we first solve the two-dimensional wave problem which is governed by Equations (2.87)-(2.91). Once this is done, we then solve the three-dimensional wave problem which is governed by Equations (3.16)-(3.21), where now α, ω and the ζ_n are known.

The three-dimensional wave problem is governed by Equations (3.16)-(3.21). In the temporal stability case, we set γ equal to zero whereas in the spatial stability case we set σ equal to zero. With α, ω, R and the ζ_n known and for a certain assumed value of the spanwise wavenumber β, Equations (3.16)-(3.21) are of the same mathematical nature as Equations (2.67)-(2.72) and they are solved in the same way which was explained in Section 4.1.4 in order to determine the eigenvalue γ in the

spatial stability case, or the eigenvalue σ in the temporal stability case. However, in order to replace the boundary conditions at $y = \infty$ with boundary conditions at some finite value of y, $y = y_{max}$, we note that for a large value of y ($y \geq y_{max}$), $U \to 1$ and $DU \to 0$ but the ζ_n are functions of y and are not constants. This means that for $y \geq y_{max}$, and due to the interaction terms (the underlined terms in Equations (3.16)-(3.21)), we don't get a system of equations with constant coefficients which was the case in Section 4.1.4. To overcome this difficulty we note that the interaction terms are of order $A_o\zeta\psi$ whereas the rest is of order ψ. Since the ζ_n and the ψ_n vanish as $y \to \infty$, Then the interaction terms decay faster than the rest of the terms. Thus by choosing a large enough y_{max}, the interaction terms can be neglected when we derive the boundary conditions at $y = y_{max}$. The error involved can be monitored by choosing a certain value of y_{max} and solving the problem, then increasing y_{max} and solving the problem again and noting the effect of increasing y_{max} on the accuracy of the solution.

CHAPTER V

RESULTS AND CONCLUSIONS

In this chapter we introduce and discuss results from both the resonant triad model and the Floquet theory model. The results introduced are for the spatial quasi-parallel case.

Most of the parameters considered correspond to those in the controlled experiment of Kachanov and Levchenko [9]. The non-dimensional frequency ω is given by

$$\omega = \omega^* \frac{\delta_r^*}{U_\infty^*}$$

where ω^* is the dimensional circular frequency and δ_r^* is defined in Equation (2.48). Using Equation (2.30) in the above equation we have

$$\omega = \frac{\omega^* \nu^*}{U_\infty^{*2}} R$$

Since $\omega^* = 2\pi f^*$, the above equation becomes

$$\omega = \frac{2\pi f^* \nu^*}{U_\infty^{*2}} R$$

So, we let

$$\omega = FR \tag{5.1}$$

where

$$F = \frac{2\pi f^* \nu^*}{U_\infty^{*2}} \tag{5.2}$$

In the spatial stability case, which is the case we present results for, F remains constant if we follow a certain wave. The results introduced are at $F = 124 \times 10^{-6}$ which corresponds to the frequency in the controlled

experiment of Kachanov and Levchenko [9]. The non-dimensional spanwise wavenumber β is given by

$$\beta = \beta^* \delta_r^*$$

where β^* is the dimensional spanwise wavenumber. Using Equation (2.30) in the above equation we have

$$\beta = \beta^* \frac{\nu^*}{U_\infty^*} R$$

So, we let

$$\beta = \frac{bR}{1000} \tag{5.3}$$

where

$$b = 1000 \frac{\beta^* \nu^*}{U_\infty^*} \tag{5.4}$$

For a certain three-dimensional wave, b remains constant as the wave propagates downstream. Similar to the spanwise wavenumber, the streamwise wavenumber α_r is defined as

$$\alpha_r = \frac{aR}{1000} \tag{5.5}$$

where

$$a = 1000 \frac{\alpha^* \nu^*}{U_\infty^*} \tag{5.6}$$

For a certain wave, a remains almost constant as the wave propagates downstream.

5.1 Results from the Resonant Triad Model

For the spatial quasi-parallel case, the modulation equations (2.111) and (2.112) reduce to

$$H_2 \frac{dB}{dx} = - \Lambda_2 A \bar{B} \, e^{i(\theta - \theta_1 - \bar{\theta}_1)} \tag{5.7}$$

$$h_2 \frac{dA}{dx} = - \Lambda_1 B^2 e^{i(2\theta_1 - \theta)} \tag{5.8}$$

where the terms on the right-hand side are due to the interaction of the two modes. Dropping these terms decouples the two modes and yields $B = B_o$ and $A = A_o$ where B_o and A_o are the amplitudes at $R = R_1$ of the 3-D and the 2-D waves, respectively. The no-interaction amplitudes at any R are then equal to

$$B_{NI}(R) = B_o e^{-2\int_{R_1}^{R} \alpha_{1i} dR} \tag{5.9}$$

$$A_{NI}(R) = A_o e^{-2\int_{R_1}^{R} \alpha_{1i} dR} \tag{5.10}$$

Figure 5 shows the variation of the rate of growth with R for a two dimensional wave at $F = 124 \times 10^{-6}$. The two-dimensional wave remains unstable up to $R_{II} = 606$ where it becomes stable. The figure also shows the variation of the rate of growth with R for a three-dimensional wave at $F = 62 \times 10^{-6}$. At $b = 0.33$ the wave is damped over the whole range of R, whereas at $b = 0.18$ the wave remains stable up to $R = 540$ where it becomes unstable.

For a certain pair of three-dimensional waves having spanwise wavenumbers of b and -b at a frequency equal to one-half the frequency of the two-dimensional wave, the condition for perfect subharmonic resonance is

$$\alpha_{1r} = \frac{1}{2} \alpha_r$$

This condition might be satisfied at some value of R, however, when the wave propagates downstream the perfect subharmonic resonance condition

is no longer satisfied and the three-dimensional wave is detuned. The percentage of detuning is defined as

$$\sigma\% = \frac{\alpha_{1r} - \frac{1}{2}\alpha_r}{\alpha_{1r}} \times 100\% \tag{5.11}$$

The variation of the percentage of detuning with R is shown in Fig. 6. For b = 0.33 the wave is detuned over the whole considered range of R, whereas for b = 0.18 the wave is tuned at R = 596 and at R = 652, but it is detuned at all other values of R within the considered range of R. The figure also shows that at the considered frequency, the detuning of a wave having b = 0.33 is much larger than that of a wave having b = 0.18.

By allowing for the interaction of the two-dimensional wave and the pair of the three-dimensional subharmonic waves, the coefficients Λ_2 and Λ_1 in Equations (5.7) and (5.8) become non-zero. We point out here that in computing the coefficients Λ_2, H_2, Λ_1 and h_2 in Equations (5.7) and (5.8), the eigenfunctions are normalized by setting the maximum value of the magnitude of the eigenfunction corresponding to the streamwise disturbance equal to 1. That is

$$\{\max (\xi_{1r}^2 + \xi_{1i}^2)^{\frac{1}{2}}, \quad \max (\zeta_{1r}^2 + \zeta_{1i}^2)^{\frac{1}{2}}\} = \{1,1\} \tag{5.12}$$

and by setting the phase of the derivative of the eigenfunction corresponding to the streamwise disturbance at the plate equal to zero. That is

$$\{\frac{d\xi_{1i}}{dy} (y = 0), \frac{d\zeta_{1i}}{dy} (y = 0)\} = \{0,0\} \tag{5.13}$$

The variation of the ratio of the magnitude of Λ_2/H_2 to the magnitude of Λ_1/h_2 with R is shown in Fig. 7 for b = 0.33 and b = 0.18. We note from the figure that the magnitude of Λ_2/H_2 is much larger than the magnitude of Λ_1/h_2, which indicates that the interaction affects the pair of the three-dimensional waves much more than it affects the two-dimensional wave. Figure 8 shows the variation of the magnitude of Λ_2/H_2 with R for b = 0.33 and b = 0.18. The magnitude of Λ_2/H_2 is monotonically increasing with R for both spanwise wavenumbers, and is larger for b = 0.33 than for b = 0.18 at the considered frequency. The variation of the magnitude of Λ_1/h_2 with R is shown in Fig. 9, and at the considered frequency it is larger for b = 0.18 than for b = 0.33.

Equations (5.7) and (5.8) along with the initial values of A and B at some value of R are integrated to compute A and B as they vary with R. Figure 10 shows the variation with R of the maximum r.m.s. amplitudes of the two-dimensional and three-dimensional Orr-Sommerfeld subharmonic waves at b = 0.33.

In the figure the three-dimensional subharmonic wave has the same initial r.m.s. amplitude of 10^{-4}, whereas the initial r.m.s. amplitude of the two-dimensional wave has the values 5×10^{-4}, 10^{-3} and 1.3×10^{-3}. At low initial amplitudes of the two-dimensional wave (Fig. 10.a), the amplitude of the three-dimensional subharmonic wave oscillates while decaying. As the initial amplitude of the two-dimensional wave reaches a certain threshold value, the three-dimensional subharmonic wave is

eventually excited and its amplitude grows (Fig. 10.b). Increasing the initial amplitude of the two-dimensional wave further (Fig. 10.c), the amplitude of the three-dimensional subharmonic wave increases at a larger rate, and as this amplitude reaches large values, the effect of the interaction on the amplitude of the two-dimensional wave becomes appreciable and leads to the growth of the two-dimensional wave in a region where it would decay according to the standard no-interaction behavior of this wave.

A qualitatively similar kind of behavior is noticed at b = 0.18. Figure 11 shows the variation with R of the maximum r.m.s. amplitudes of the two-dimensional and the three-dimensional Orr-Sommerfeld subharmonic waves. The initial r.m.s. amplitude of the three-dimensional subharmonic wave is the same and is equal to 10^{-4}, whereas the r.m.s. amplitude of the two-dimensional wave has the values 5.0×10^{-4}, 1.8×10^{-3} and 2.1×10^{-3}. By comparing Figure 11 with Figure 10 we note that the threshold amplitude of the two-dimensional wave which excites the subharmonic is larger at b = 0.18 than at b = 0.33.

5.2 Results from the Floquet Theory Model

The parametric instability problem consisting of a two-dimensional wave governed by Equations (2.87)-(2.91) exciting with a pair of three-dimensional subharmonic waves, governed by Equations (3.16)-(3.21), is solved for the spatial case. The amplitudes A and B at any value of R are then given by

$$A(R) = A_o e^{-2\int_{R_1}^{R} \alpha_i dR} \qquad (5.14)$$

$$B(R) = B_o e^{2\int_{R_1}^{R} \gamma_r dR} \qquad (5.15)$$

where A_o and B_o are the initial amplitudes at $R = R_1$. Figure 12 shows the variation of the maximum r.m.s. amplitudes of the two-dimensional and the three-dimensional subharmonic waves with R. The maximum r.m.s. amplitude of the three-dimensional waves at R = 430 is 10^{-5}, whereas that of the two-dimensional wave at the same R is 5.2×10^{-3} in the case of b = 0.33 and 2.83×10^{-3} in the case of b = 0.18.

5.3 Comparison with Experimental Data

Kachanov and Levchenko [9] studied experimentally the three-dimensional resonant interaction of a plane T-S wave having a frequency f_1 with a pair of oblique waves having the frequency $\frac{1}{2} f_1$. In the controlled part of the experiment, the frequency f_1 is equal to 111.4 Hz, which corresponds to $F = 124\times10^{-6}$, the spanwise wavenumber β^* is equal to 0.195 mm^{-1} which corresponds to b = 0.33. The amplitudes of the waves are measured at

$$\frac{y^*}{\text{boundary-layer thickness}} = 0.26$$

where the boundary-layer thickness is determined experimentally from the condition $U^*/U^*_\infty = 0.99$. This corresponds to measuring the amplitudes of the waves at y = 1.3.

Figure 13 shows the streamwise variation of the r.m.s. amplitude of the two-dimensional wave and the three-dimensional subharmonic wave as predicted by the Floquet theory model compared with the experimental

data. The theoretical and the experimental amplitudes are at y = 1.3. The initial amplitude of the three-dimensional subharmonic wave was chosen such that the theoretical and the experimental amplitudes match at R_{II} = 606. The agreement is very good.

The y variation of the magnitude and phase of the eigenfunction of the streamwise disturbance at R_{II} = 606 as predicted by the Floquet theory model is shown in Fig. 14; they are compared with the experimental data at R = 608.

Figures 15 and 16 are like Figs. 13 and 14, but they compare results predicted by the resonant triad model at b = 0.33 with the corresponding experimental data.

Figure 17 compares the results predicted by the resonant triad model at b = 0.18 with the experimental data for which b = 0.33.

5.4 Discussion

In the parametric instability formulation, which was presented in Chapter III, the subharmonic instability problem is viewed as a secondary instability problem. The basic flow is a superposition of the Blasius profile and a two-dimensional wave which is almost periodic in the streamwise direction. The periodicity of the basic flow and the guidence of Floquet theory suggest the form of the solution given by Equations (3.14) and (3.15). Using the form we end up with Equations (3.16)-(3.21). In this formulation few assumptions are made. First, the mean flow and the disturbances are assumed to be quasi-parallel. For amplitudes of the two-dimensional wave which are larger than the

threshold amplitude necessary to excite the subharmonic, the nonparallel effect on the rate of growth of the subharmonic might be small compared with the large values of the rate of growth of the subharmonic. However, the nonparallel effects on the wavenumber and the rate of growth of the two-dimensional wave might be more important; the importance being that the rate of growth of the subharmonic seems to be a strong function of the amplitude of the two-dimensional wave. The resonant triad model, on the other hand, relaxes the quasi-parallel assumption and accounts for the weakly nonparallel effects. A second assumption which is made in the parametric instability model is that the two-dimensional wave affects the subharmonic, but it is not affected itself by the interaction. This assumption seems to be reasonable as long as the amplitude of the subharmonic is not too large. As we have seen from the results of the resonant triad model, which accounts for the effect of the interaction on the two-dimensional wave, the amplitude of the two-dimensional wave deviates from the linear no-interaction behavior as the amplitude of the subharmonic reaches large values. This behavior was noted in the natural disturbance experiments [9]. It is however important to note that as the amplitude of the subharmonic reaches large values and the frequency spectrum tends to become filled with growing disturbances, the validity of any of the two models is questionable. A third assumption which is made in the parametric instability model is to restrict the effect of the spatially dependent quantity $A_o e^{-\int \alpha_i dx}$ in Equations (3.16)-(3.19) to be local and thus treat

it in the equations as a constant. This assumption is justified by the weak spatial dependence of $A_o e^{-\int \alpha_i dx}$.

One problem that the parametric instability model seems not to do much about is to introduce a clear understanding of the link between the subharmonic mode and the different three-dimensional Tollmien-Schlichting modes. Herbert [33] found that the Orr-Sommerfeld modes and Squire modes are inherent parts of the eigenvalue spectrum for three-dimensional disturbances as the amplitude of the two-dimensional wave goes to zero. However, this does not answer the question of how does the subharmonic orginate from the three-dimensional Tollmien-Schlichting modes, and the resonant triad model or some rational modification of it might be more promising in introducing such an important understanding.

Despite the assumptions discussed above, the parametric instability model gives results which are in a better agreement with the experimental data than those we obtain from the resonant triad model. In the resonant triad model we start with a two-dimensional Tollmien-Schlichting wave and a pair of spanwise symmetric three-dimensional Tollmien-Schlichting modes having a wavenumber which is close to one-half the wavenumber of the two-dimensional wave. The effect of the interaction is to modify the amplitudes and the wavenumbers of the interacting waves. The interaction problem in this sense is viewed as a higher-order problem in a perturbation sequence of problems. This idea looks clearer if the problem is formulated using the method of multiple scales [26,37,47], rather than the method of averaging which is used in this study. Viewing the interaction this way restricts the range of the

validity of the resonant triad model by putting limitations on the strength of the interaction. Another point, which is related to the above discussion, is that in the resonant triad model the mode shapes of the interacting waves are slightly perturbed as a result of the interaction. It seems from the experimental data and the results of the parametric instability model that the mode shape as well as the amplitude and the wavenumber of the subharmonic are greatly modified as a result of the interaction. Figure 18 compares the subharmonic mode eigenfunctions of u, v, p and w computed using the parametric instability model with those of the three-dimensional Tollmien-Schlichting Orr-Sommerfeld mode used in the resonant triad model under the conditions of a strong interaction. It is clear from the figure that representing the subharmonic eigenfunctions by the eigenfunctions of a single Orr-Sommerfeld mode is not very successful in the presence of a strong interaction. This leads us to think of the idea of representing the subharmonic mode by more than one three-dimensional Tollmien-Schlichting mode. This seems like a rational thing to do, and it might be important to include the Squire modes as well as the Orr-Sommerfeld modes, especially with the finding from the parametric instability model [48] that tracing the principal eigenvalue to the limit as the amplitude of the two-dimensional wave goes to zero has shown that in a large band of spanwise wavenumbers, the subharmonic secondary instability is linked to eigensolutions of Squire's equation. However, it is not very clear how to determine the

contribution of each mode to the subharmonic and how to carry the analysis on a rational basis.

With the above discussion in mind, it seems that the discrepancy between the results of the resonant triad and the experimental data is mainly because the amplitude of the two-dimensional wave in the experiment is large and consequently the interaction is so strong that the validity of the resonant triad model is doubted.

So far it was shown that there is a problem with the resonant triad model in the presence of a strong interaction, so if that is the only major problem then we expect to obtain more reasonable predictions from the resonant triad model if we have a weak interaction. In the limit as the amplitude of the two-dimensional wave goes to zero both the parametric instability model and the resonant triad model give identical results. For small amplitudes of the two-dimensional wave we expect the results from the two models to get close to each other. Figure 19 compares the variation with R of the maximum r.m.s. amplitudes of the two-dimensional and three-dimensional Orr-Sommerfeld subharmonic mode, as predicted by the resonant triad model, with the predictions of the parametric instablity model. However, the final evaluation of the resonant triad model in the presence of a weak interaction might not be possible until an experiment with such a weak interaction is performed.

5.5 Conclusions

In this study the subharmonic instability in the two-dimensional boundary layer on a flat plate has been analyzed using the parametric

instability model and the resonant triad model. The problems arising from both models have been solved numerically using a shooting technique and results have been presented. The two models have been evaluated based on discussing the assumptions underlying them, comparison of the results with experimental data, and how the results from both models compare with each other. Based on this study it is concluded that

i) Both models show that the amplitude of the two-dimensional wave should exceed a certain threshold value for the subharmonic mode to be excited. This threshold amplitude is relatively small.

ii) The parametric instability model does not account for the nonparallel effects and the effect of the interaction on the two-dimensional wave. The model also assumes that the spatial dependence of the amplitude of the two-dimensional wave affects the subharmonic mode only locally.

iii) The results from the parametric instability model are in a very good agreement with the experimental data. This sets the model as a powerful one even in the presence of a strong interaction.

iv) The parametric instability model does not answer the question of how does the subharmonic mode originate from the three-dimensional Tollmien-Schlichting modes. The resonant triad model or some

modified or generalized form of it is more promising in this regard.

v) The resonant triad model shows that at large amplitudes of the subharmonic mode, the development of the two-dimensional wave deviates from a linear behavior. The interaction might cause the amplitude to grow in a region where it would decay according to the linear behavior. This kind of behavior was noted in the natural disturbance experiment [9].

vi) The resonant triad model is a weakly nonlinear model, which is not valid in the presence of strong interactions.

vii) The parametric instability model shows that the shapes of the eigenfunctions of the subharmonic mode are not exactly as those of the three-dimensional Tollmien-Schlichting waves. The difference is due to the interaction. The resonant triad model fails to account for this difference, and the error introduced because of this failure seems to be large in the presence of a strong interaction.

viii) The results from the resonant triad model agree only qualitatively with the experimental data. The discrepancy seems to be due to the large amplitudes of the two-dimensional wave in the experiment,

which causes a strong interaction, and thus the resonant triad model is questionable at such a strong interaction.

ix) The resonant triad model is numerically less demanding than the parametric instability model.

x) As the amplitude of the two-dimensional wave gets smaller and smaller, results from both models get closer to each other. As the amplitude goes to zero, the two models become identical.

REFERENCES

1. Klebanoff, P. S. and Tidstrom, K. D., "Evolution of Amplified Waves Leading to Transition in a Boundary Layer with Zero Pressure Gradient," NASA Technical Note, No. D-195, 1959.

2. Klebanoff, P. S., Tidstrom, K. D. and Sargent, L. M., "The Three-Dimensional Nature of Boundary-Layer Instability," Journal of Fluid Mechanics, Vol. 12, 1962, pp. 1-34.

3. Kovasznay, L. S. G., Komoda, H. and Vasudeva, B. R., "Detailed Flow Field in Transition," Proceedings of the 1962 Heat Transfer and Fluid Mechanics Institute, 1962, pp. 1-26.

4. Nishioka, M., Asai, M. and Iida, S., "An Experimental Investigation of the Secondary Instability," Laminar-Turbulent Transition: Proceedings of the IUTAM Symposium, Stuttgart (eds. R. Eppler and H. Fasel), Springer-Verlag, Berlin, 1980, pp. 37-46.

5. Nishioka, M., Iida, S. and Ichikawa, Y., "An Experimental Investigation of the Stability of Plane Poiseuille Flow," Journal of Fluid Mechanics, Vol. 72, 1975, pp. 731-751.

6. Nishioka, M., Iida, S. and Kanbayashi, S., "An Experimental Investigation of the Subcritical Instability in Plane Poiseuille Flow," Proceedings of the 10th Turbulence Symposium, Institute Space Aeronautical Sciences, Tokyo University, 1978, pp. 55-62.

7. Nishioka, M. and Asai, M., "Three-Dimensional Wave-Disturbances in Plane Poiseuille Flow," Laminar-Turbulent Transition: Proceedings of the IUTAM Symposium, Novosibirsk (eds. V. V. Kozlov), 1985, pp. 173-182.

8. Kachanov, Yu. S., Kozlov, V. V. and Levchenko, V. Ya., "Nonlinear Development of a Wave in a Boundary Layer," Fluid Dynamics, Vol. 3, 1977, pp. 383-390. [trs. of Mekh. Zhid. i Gaza 3, 49-53].

9. Kachanov, Yu. S. and Levchenko, V. Ya., "The Resonant Interaction of Disturbances at Laminar-Turbulent Transition in a Boundary Layer," Journal of Fluid Mechanics, Vol. 138, 1984, pp. 209-247.

10. Kachanov, Yu. S., Kozlov, V. V., Levchenko, V. Ya. and Ramazanov, M. P., "On the Nature of K-Breakdown of a Laminar Boundary Layer. New Experimental Data," Laminar-Turbulent Transition: Proceedings of the IUTAM Symposium, Novosibirsk (ed. V. V. Kozlov), 1985, pp. 61-73.

11. Komoda, H., "Nonlinear Development of Disturbances in a Laminar Boundary Layer," Physics of Fluids, Suppl., Vol. 10, 1967, pp. 587-594.

12. Williams, D. R., Fasel, H., and Hama, F. R., "Experimental Determination of the Three-Dimensional Vorticity Field in the Boundary-Layer Transition Process," Journal of Fluid Mechanics, Vol. 149, 1984, pp. 179-203.

13. Hama, F. R., Long, J. D. and Hegarty, J. C., "On Transition from Laminar to Turbulent Flow," Journal of Applied Physics, Vol. 28, 1957, p. 388.

14. Hama, F. R., "Boundary-Layer Transition Induced by a Vibrating Ribbon on a Flat Plate", Proceedings 1960 Heat Transfer and Fluid Mechanics Institute, Stanford University Press, 1960, pp. 92-105.

15. Hama, F. R. and Nutant, J., "Detailed Flow-Field Observations in the Transition Process in a Thick Boundary Layer," Proceedings of the 1963 Heat Transfer and Fluid Mechanics Institute, 1963, pp. 77-93.

16. Wortmann, F. Z., "The Incompressible Fluid Motion Downstream of Two-Dimensional Tollmien-Schlichting Waves," Laminar-Turbulent Transition, Proceedings of the AGARD Conference No. 224, Lyngby, Denmark, Paper 12, 1977.

17. Saric, W. S. and Thomas, A. S. W., "Experiments on the Subharmonic Route to Turbulence in Boundary Layers," Turbulence and Chaotic Phenomena in Fluids, Proceedings of the IUTAM Symposium, Kyoto (ed. T. Tatsumi). North Holland, 1984.

18. Kozlov, V. V. and Ramazanov, M. P., "Development of Finite-Amplitude Disturbances in Poiseuille Flows," Journal of Fluid Mechanics, Vol. 147, 1984, pp. 149-157.

19. Schubauer, G. B. and Skramstad, H. K., "Laminar Boundary Layer Oscillations on a Flat Plate," NACA Rep. No. 909, 1948.

20. Fales, E. N., "A New Laboratory Technique for Investigation of the Origin of Fluid Turbulence," Journal of Franklin Institute, Vol. 259, 1951, p. 491.

21. Weske, J. R., "Experimental Study of Detail Phenomena of Transition in Boundary Layers," University of Maryland Technical Note, 1957, No. BN-91.

22. Corke, T. C. and Mangano, R. A., "Transition of a Boundary Layer: Controlled Fundamental-Subharmonic Interactions," Bulletin of the American Physical Society, Vol. 31, 1986.

23. Raetz, G. S., "A New Theory of the Case of Transition in Fluid Flows," Norair Rep, NOR-59-383. Hawthorne, CA, 1959.

24. Raetz, G. S., "Current Status of Resonance Theory of Transition," Norair Rep. NOR-64-111. Hawthorne, CA, 1964.

25. Stuart, J. T., "On Three-Dimensional Non-Linear Effects in the Stability of Parallel Flows," Advances in Aerospace Sciences, Vol, 3, 1961, pp. 121-142.

26. Lekoudis, S. G., "Resonant Wave Interactions on a Swept Wing," AIAA Journal, Vol. 18, 1980, pp. 122-124.

27. Craik, A. D. D., "Nonlinear Resonant Instability in Boundary Layers," Journal of Fluid Mechanics, Vol. 50, 1971, pp. 393-413.

28. Craik, A. D. D., "Second Order Resonance and Subcritical Instability," Proceedings of the Royal Society, London, Vol. A343, 1975, pp. 351-362.

29. Craik, A. D. D., "Evolution in Space and Time of Resonant Wave Triads. II. A Class of Exact Solutions," Proceedings of the Royal Society, London, Vol. A363, 1978, pp. 257-269.

30. Lekoudis, S. G., "On the Triad Resonance in the Boundary Layer," Lockheed-Georgia Company Report No. LG77ER0152, 1977.

31. Kelly, R. E., "On the Stability of an Inviscid Shear Layer which is Periodic in Space and Time," Journal of Fluid Mechanics, Vol. 27, pp. 657-689, 1967.

32. Maseev, L. M., "Occurrence of the Three-Dimensional Perturbations in Boundary Layers," Fluid Dynamics, Vol. 3, pp.23-24, 1968.

33. Herbert, Th., "Analysis of the Subharmonic Route to Transition in Boundary Layers," Paper No. 84-0009, 1984.

34. Herbert, Th., "Secondary Instability of Shear Flows," In AGARD-R-709, 1984.

35. Herbert, Th., "Three-Dimensional Phenomena in the Transitional Flat-Plate Boundary Layer," AIAA Paper 85-0489, 1985.

36. Nayfeh, A. H., "Nonlinear Stability of Boundary Layers," AIAA Paper 87-0044, 1987.

37. Nayfeh, A. H. and Bozatli, A. N., "Secondary Instability in Boundary-Layer Flows," Physics of Fluids, Vol. 22, pp 805-813, 1979.

38. Usher, J. R. and Craik, A. D. D., "Nonlinear Wave Interactions in Shear Flows, Part 1. A Variational Formulation," Journal of Fluid Mechanics, Vol. 66, pp. 209-221, 1974.

39. Usher, J. R. and Craik, A. D. D., "Nonlinear Wave Interactions in Shear Flows, Part 2. Third-Order Theory, " Journal of Fluid Mechanics, Vol. 70, pp. 437-461, 1975.

40. Scott, M. R. and Watts, H. A., "Computational Solution of Linear Two-Point Boundary Value Problem via Orthonormalization," SIAM Journal of Numerical Analysis, Vol. 14, pp. 40-70, 1977.

41. Bouthier, M., "Stabilite Lineaire Des Ecoulements Presque Paralleles," Journal de Mecanique, Vol. 11, pp. 599-621, 1972.

42. Bouthier, M., "Stabilite Lineaire Des Ecoulements Presque Paralleles, II. La couche Limite De Blasius," Journal de Mecanique, Vol. 12, pp. 75-95, 1973.

43. Gaster, M., "On the Effects of Boundary-Layer Growth on Flow Stability," Journal of Fluid Mechanics, Vol. 66, pp. 465-480, 1974.

44. Nayfeh, A. H., Saric, W. S., and Mook, D. T., "Stability of Non-Parallel Flows," Archives of Mechanics, Vol. 26, pp. 401-406, 1974.

45. Saric, W. S. and Nayfeh, A. H., "Non-Parallel Stability of Boundary Layer Flows," Physics of Fluids, Vol. 18, pp. 945-950, 1975.

46. Saric, W. S. and Nayfeh, A. H., "Nonparallel Stability of Boundary Layers with Pressure Gradients and Suction," in AGARD Conference Proceedings, No. 224, NATO, Paris.

47. Nayfeh, A. H., "Three-Dimensional Spatial Secondary Instability in Boundary-Layer Flows," AIAA Paper No. 85-1697, 1985.

48. Herbert, T., Bertolotti, F., and Santos, G. R., "Floquet Analysis of Secondary Instability in Shear Flows," ICASE/NASA Workshop, 1985.

49. Volodin, A. G. and Zel'man, M. B., "Three-Wave Resonance Interaction of Disturbances in a Boundary Layer," Fluid Mechanics, Vol. 13, pp. 698-703, 1979. [trs. of Mekh. Zhid. i Gaza 5, 78-84].

APPENDIX A

$$H_1 = \int_0^\infty (\xi_1^* \xi_1 + \xi_3^* \xi_3 + \xi_5^* \xi_5) dy$$

$$H_2 = \int_0^\infty [\xi_4^* \xi_1 + \xi_1^* (U\xi_1 + \xi_4) + \xi_3^* U \xi_3 + \xi_5^* U \xi_5] dy$$

$$H_4 = \int_0^\infty \left[\xi_4^* \frac{\partial \xi_1}{\partial x} + \xi_1^* \left(U \frac{\partial \xi_1}{\partial x} + \frac{\partial \xi_4}{\partial x} + \frac{\partial U}{\partial x} \xi_1 + VD\xi_1\right)\right.$$

$$\left. + \xi_3^* \left(U \frac{\partial \xi_3}{\partial x} + VD\xi_3 + \xi_3 DV\right) + \xi_5^* \left(U \frac{\partial \xi_5}{\partial x} + VD\xi_5\right)\right] dy$$

$$\Lambda_2 = \int_0^\infty [\xi_1^* \{i(\alpha - \bar{\alpha}_1)\zeta_1 \bar{\xi}_1 + \zeta_3 D\bar{\xi}_1 + \bar{\xi}_3 D\zeta_1\}$$

$$+ \xi_3^* \{i\alpha\zeta_3 \bar{\xi}_1 - i\bar{\alpha}_1 \zeta_1 \bar{\xi}_3 + \zeta_3 D\bar{\xi}_3 + \bar{\xi}_3 D\zeta_3\}$$

$$+ \xi_5^* \{\zeta_3 D\bar{\xi}_5 - i\bar{\alpha}_1 \zeta_1 \bar{\xi}_5\}] dy$$

$$h_1 = \int_0^\infty [\zeta_1^* \zeta_1 + \zeta_3^* \zeta_3) dy$$

$$h_2 = \int_0^\infty [\zeta_4^* \zeta_1 + \zeta_1^* (U\zeta_1 + \zeta_4) + \zeta_3^* U \zeta_3] dy$$

$$h_4 = \int_0^\infty [\zeta_4^* \frac{\partial \zeta_1}{\partial x} + \zeta_1^* (U \frac{\partial \zeta_1}{\partial x} + \frac{\partial \zeta_4}{\partial x} + \frac{\partial U}{\partial x} \zeta_1$$

$$+ VD\zeta_1) + \zeta_3^* (U \frac{\partial \zeta_3}{\partial x} + VD\zeta_3 + \zeta_3 DV)] dy$$

$$\Lambda_1 = 2 \int_0^\infty [\zeta_1^* (i\alpha_1 \xi_1^2 + \xi_3 D\xi_1 - \beta \xi_1 \xi_5)$$

$$+ \zeta_3^* (i\alpha_1 \xi_1 \xi_3 + \xi_3 D\xi_3 - \beta \xi_3 \xi_5)] dy$$

APPENDIX B

$$f_{12} = f_{16} = 1$$

$$f_{21} = f_{65} = \Lambda$$

$$f_{23} = RDU$$

$$f_{24} = i\alpha_1 R$$

$$f_{31} = - i\alpha_1$$

$$f_{35} = - \beta$$

$$f_{42} = - \frac{i\alpha_1}{R}$$

$$f_{43} = - \frac{\Lambda}{R}$$

$$f_{46} = -\frac{\beta}{R}$$

$$f_{64} = -\beta R$$

The rest of the elements are zero.

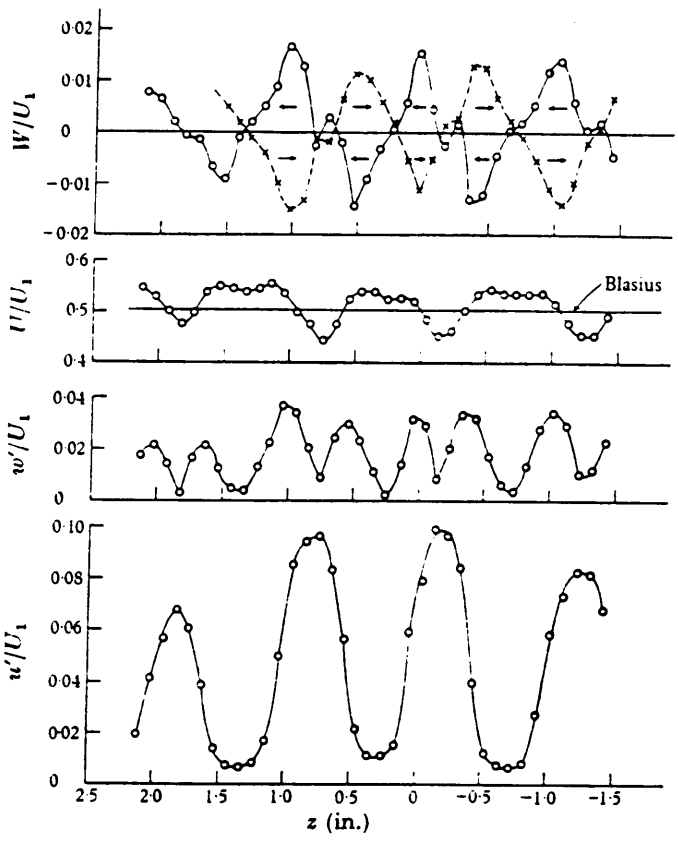

Figure 1. Spanwise distributions of mean and fluctuating components of velocity: 145 c/s wave, $U_1/\nu = 3.1 \times 10^5 ft^{-1}$. ——, $y = 0.31\ \delta$; ----, $y = 0.11\ \delta$. (Ref. 2).

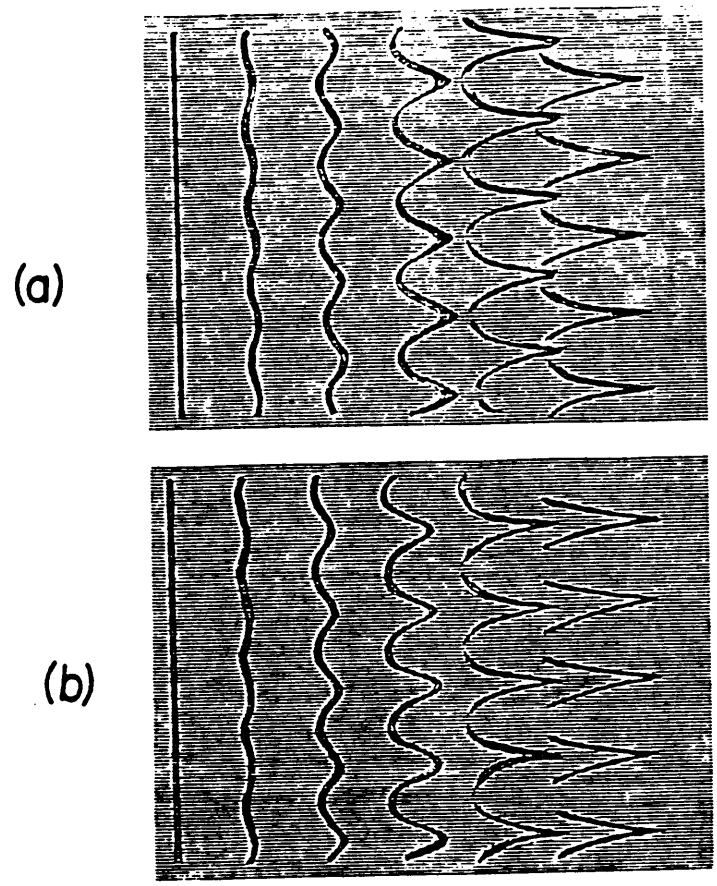

Figure 2. Streaklines in Blasius boundary layer. The drawings are a reproduction of photos taken by Saric et al. at the VPI Stability Wind Tunnel. Flow is from left to right, (a) subharmonic disturbance, (b) fundamental disturbance.

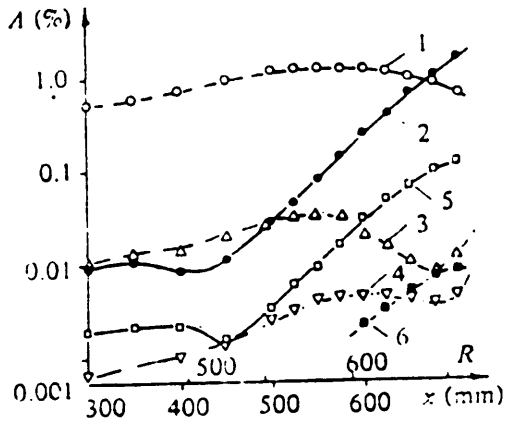

Figure 3. Amplification curves. The experiment at controlled conditions; 1,2,3,4,5,6 for f_1, $\frac{1}{2} f_1$, $2f_1$, $3f_1$, $\frac{3}{2} f_1$, $\frac{5}{2} f_1$. Principal regime, $y/\delta = 0.26$, $z = -2.5$mm. (Ref. 9).

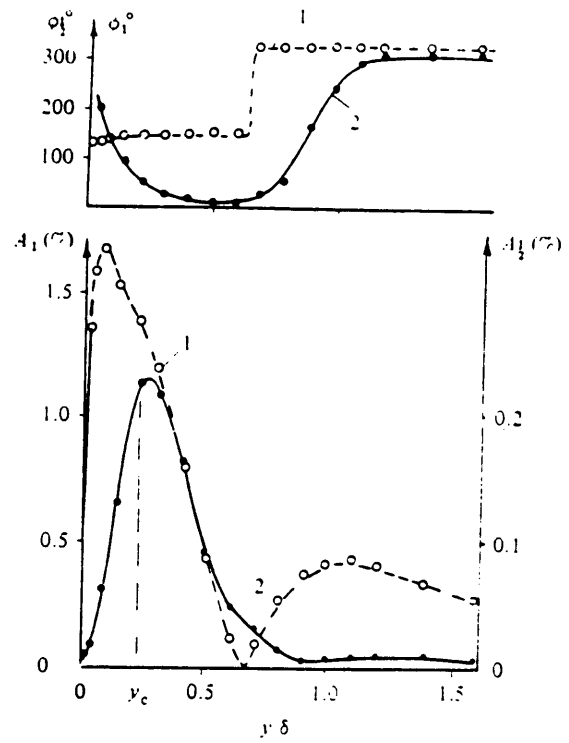

Figure 4. y-profiles of amplitudes and phases for fundamental wave (1) and subharmonic (2) at controlled conditions. Principal regime. x = 600mm (R = 608), z = - 2.5mm. (Ref. 9).

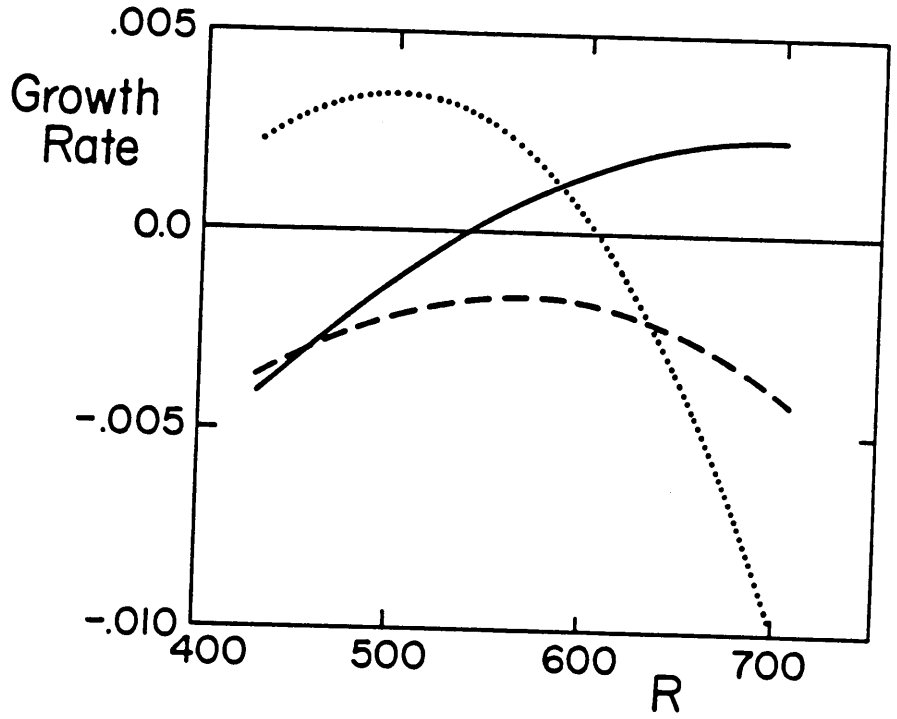

Figure 5. Variation of the rate of growth with R in the absence of interaction. ····, 2-D wave at $F = 124 \times 10^{-6}$; ——, 3-D O-S mode at $F = 62 \times 10^{-6}$ and $b = 0.18$; (----), 3-D O-S mode at $F = 62 \times 10^{-6}$ and $b = 0.33$.

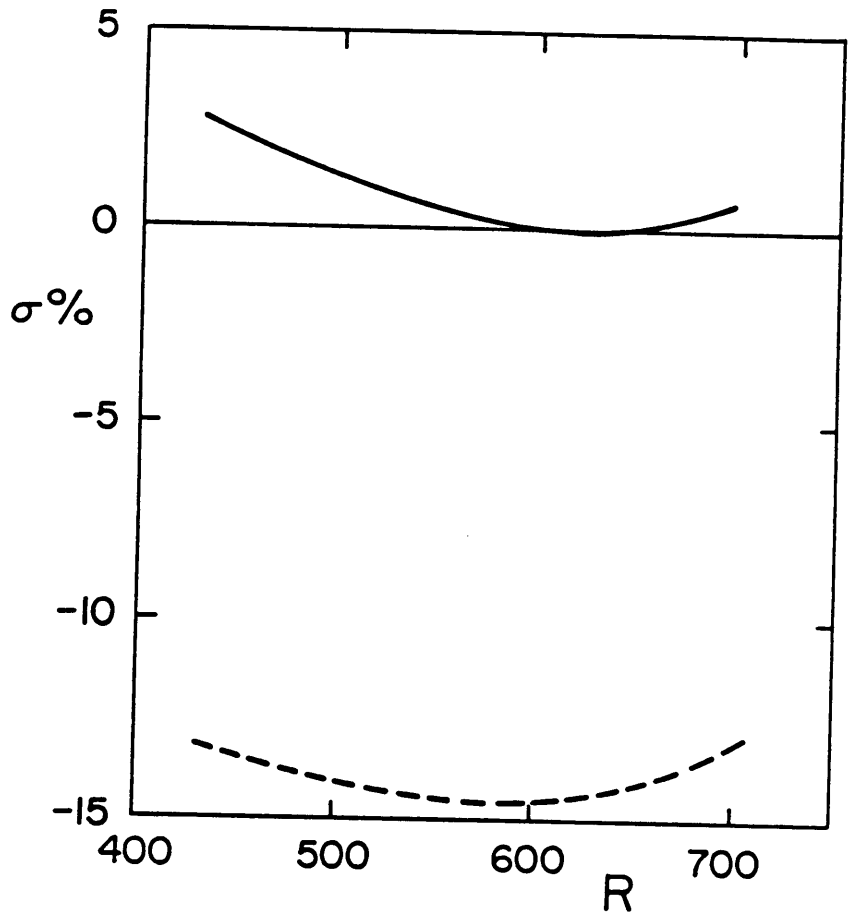

Figure 6. Variation of the percentage of detuning of the 0-S subharmonic mode with R at $F_{20} = 124 \times 10^{-6}$. b = 0.18; ----, b = 0.33.

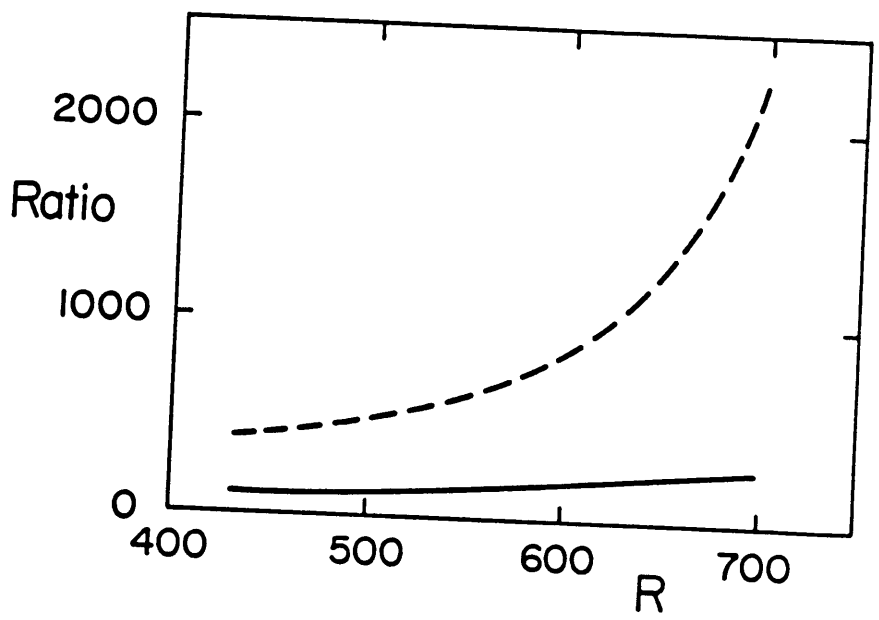

Figure 7. Variation of the ratio of the magnitude of Λ_2/H_2 to the magnitude of Λ_1/h_2 with R at $F_{2D} = 124 \times 10^{-6}$. (——), b = 0.18;(----), b = 0.33.

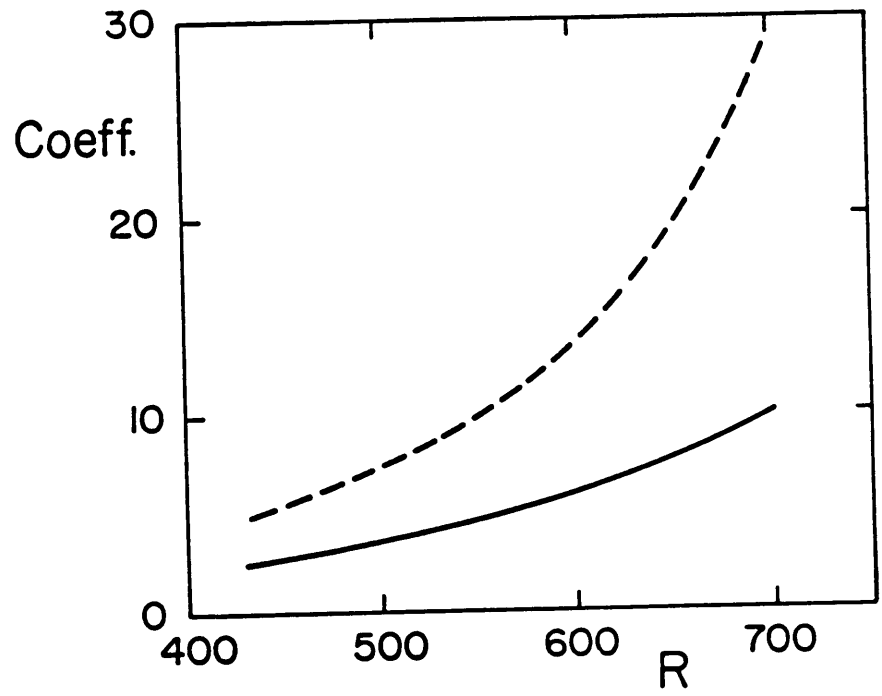

Figure 8. Variation of the magnitude of Λ_2/H_2 with R at F_{2D} = 124×10^{-6}. ——, b = 0.18; ----, b = 0.33.

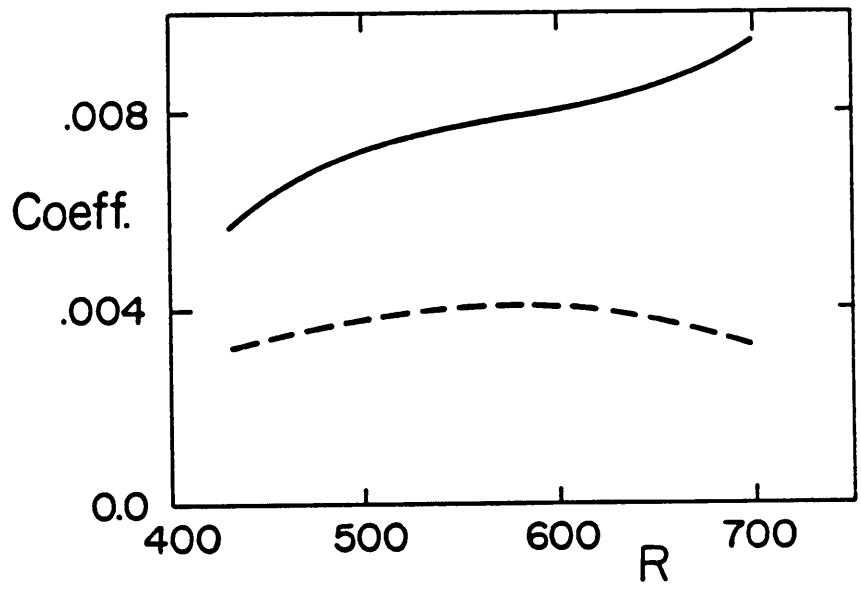

Figure 9. Variation of the magnitude of Λ_1/h_2 with R at F_{2D} = 124×10^{-6}. ——, b = 0.18; ----, b = 0.33.

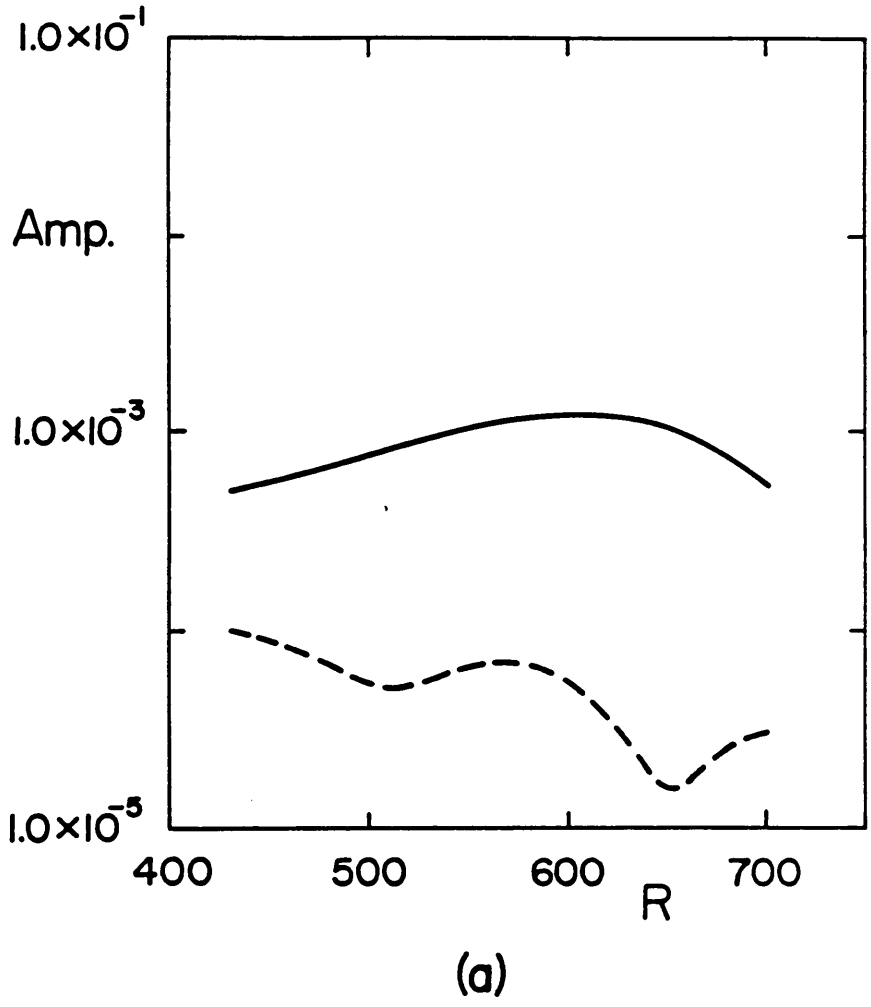

Figure 10. Variation with R of the maximum r.m.s. amplitudes of the 2-D (——) and the 3-D O-S subharmonic (----) waves. Results from the resonant triad model at $F_{2D} = 124 \times 10^{-6}$ and b = 0.33. At R = 430 the maximum r.m.s. amplitude of the 3-D wave is 10^{-4} and that of the 2-D wave is (a) 5×10^{-4}, (b) 10^{-3}, (c) 1.3×10^{-3}.

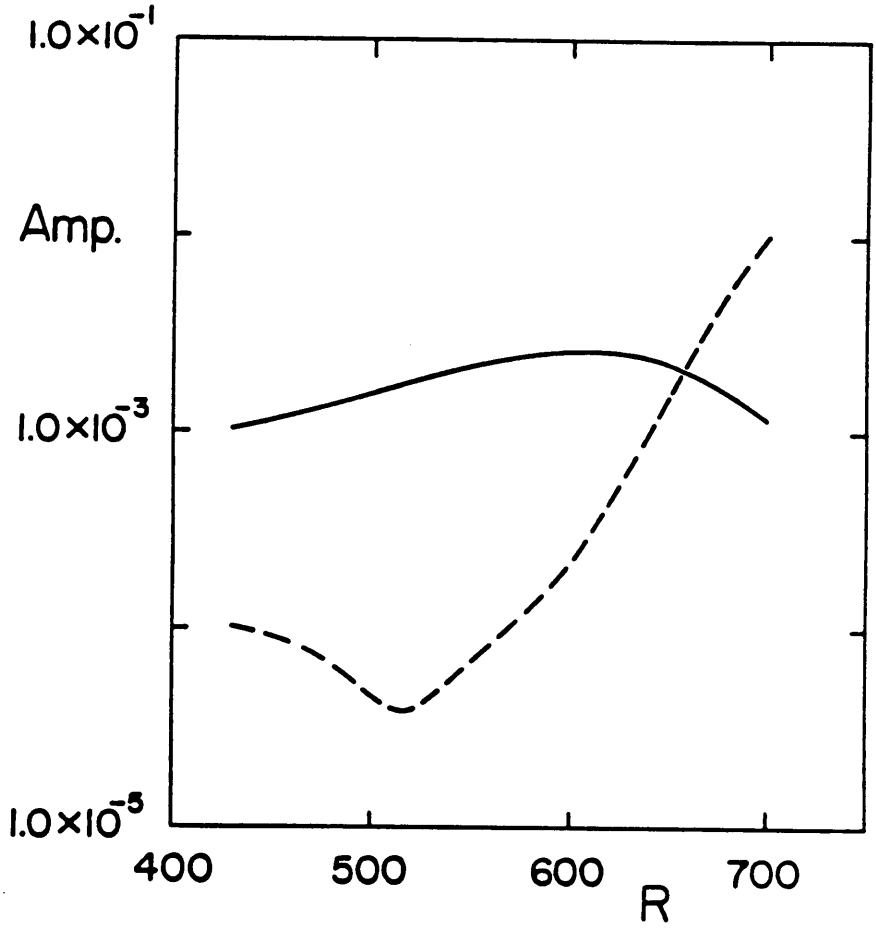

(b)

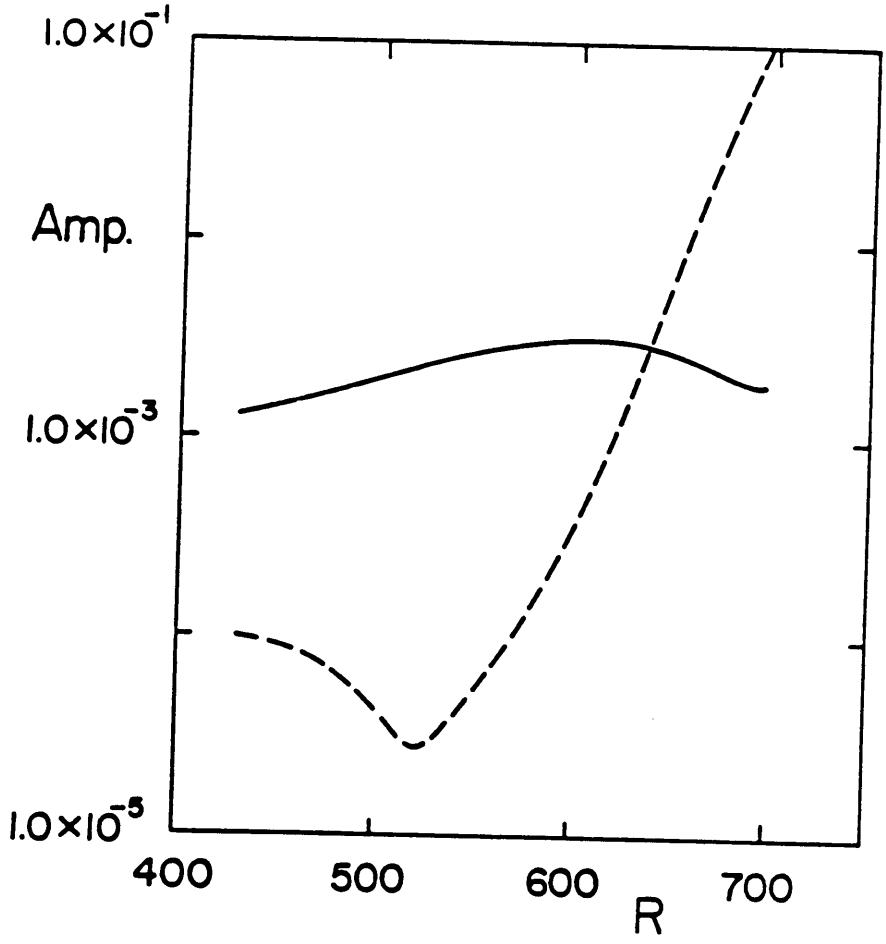

(c)

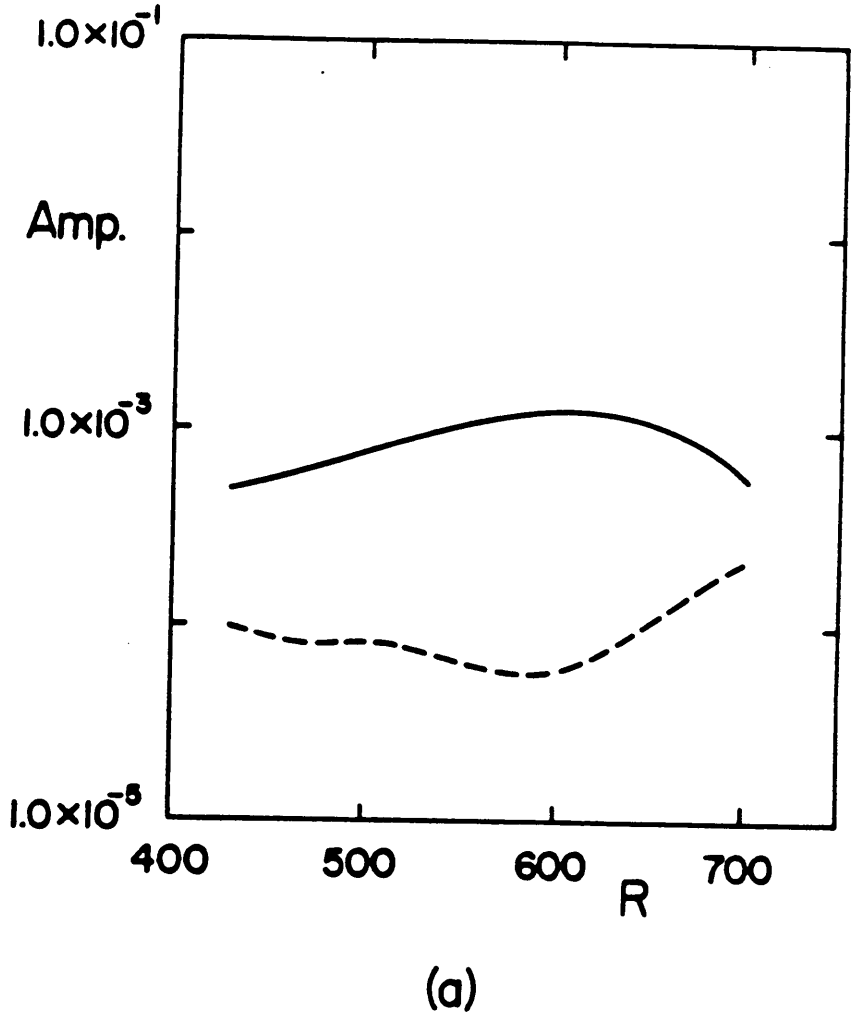

Figure 11. Variation with R of the maximum r.m.s. amplitudes of the 2-D (——) and the 3-D O-S subharmonic (----) waves. Results from the resonant triad model at $F_{2D} = 124 \times 10^{-6}$ and b = 0.18. At R = 430 the maximum r.m.s. amplitude of the 3-D wave is 10^{-4} and that of the 2-D wave is (a) 5.0×10^{-4}, (b) 1.8×10^{-3}, (c) 2.1×10^{-3}.

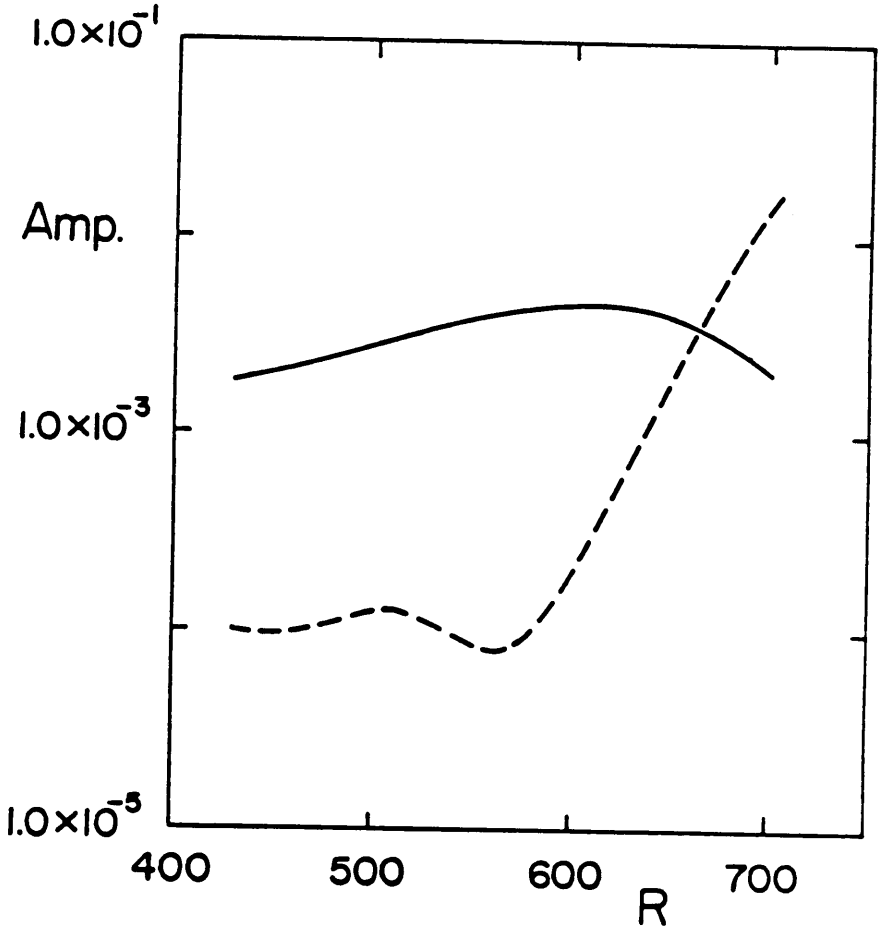

(b)

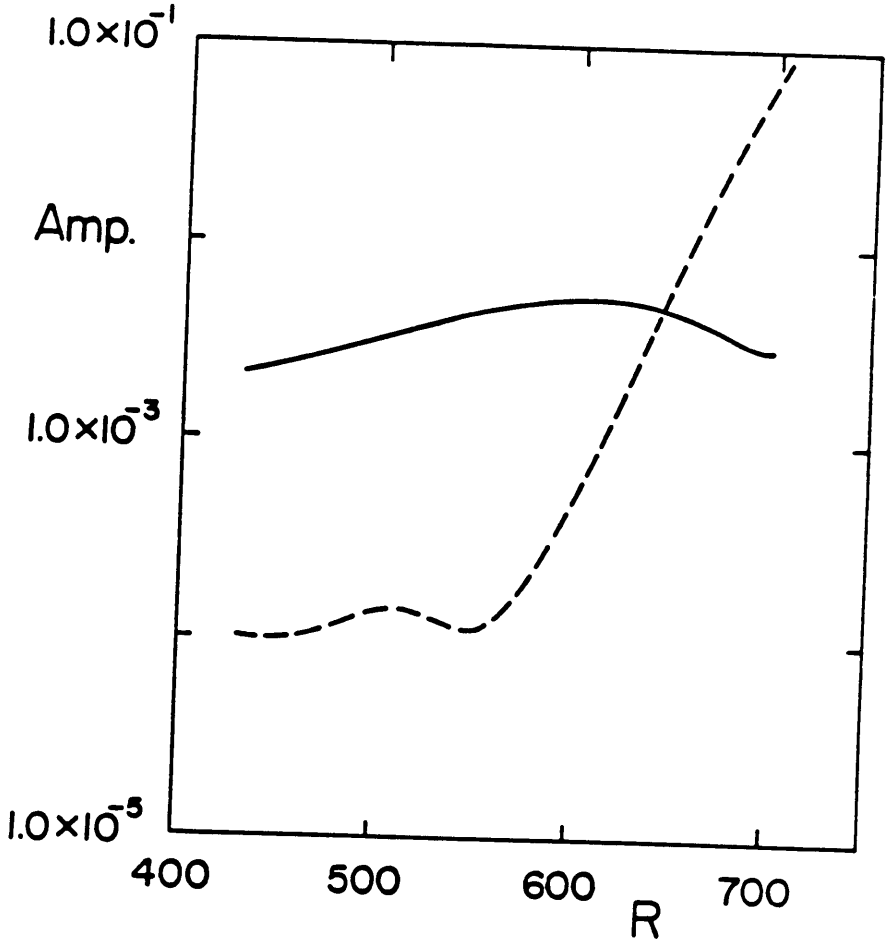

(c)

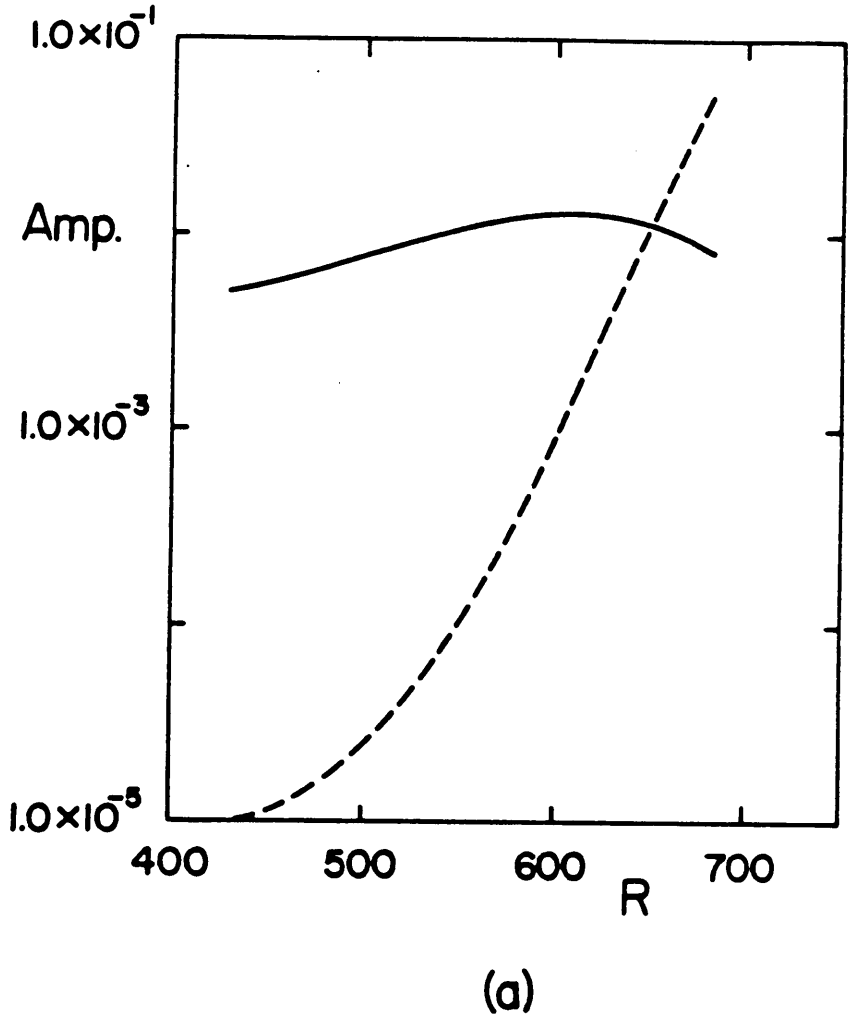

Figure 12. Variation with R of the maximum r.m.s. amplitudes of the 2-D (——) and the 3-D subharmonic (----) waves. Results from the Floquet theory model at $F_{2D} = 124 \times 10^{-6}$. At R = 430 the maximum r.m.s. amplitude of the 3-D wave is 10^{-5} and of the 2-D wave is (a) 5.2×10^{-3}, b = 0.33 and (b) 2.83×10^{-3}, b = 0.18.

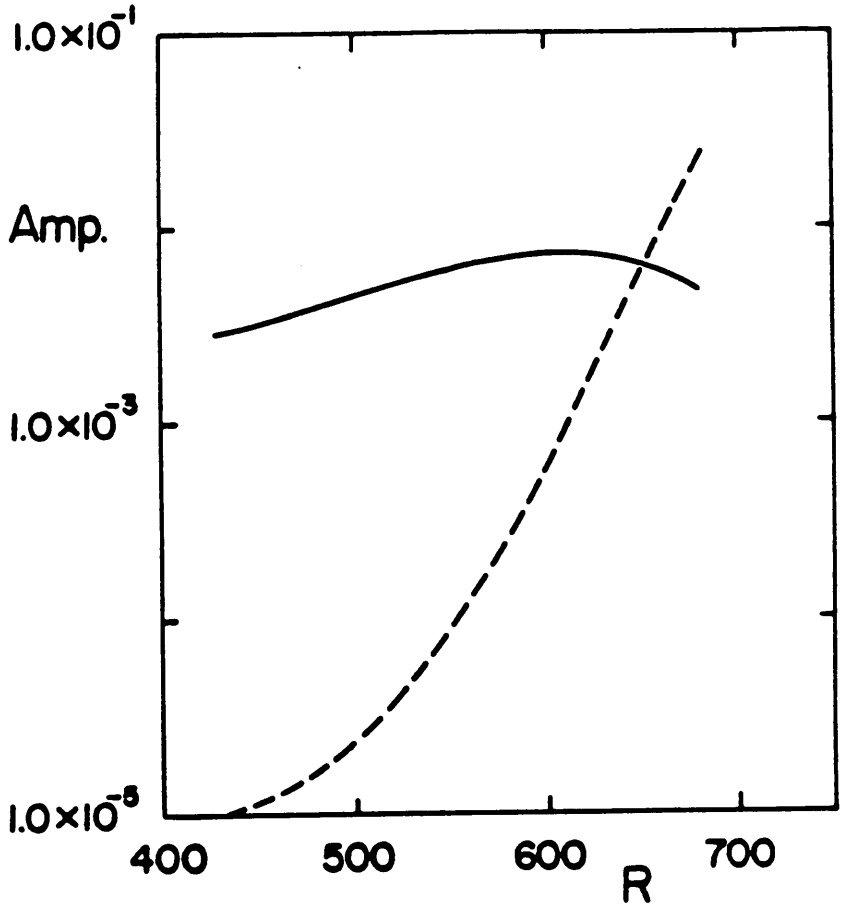

(b)

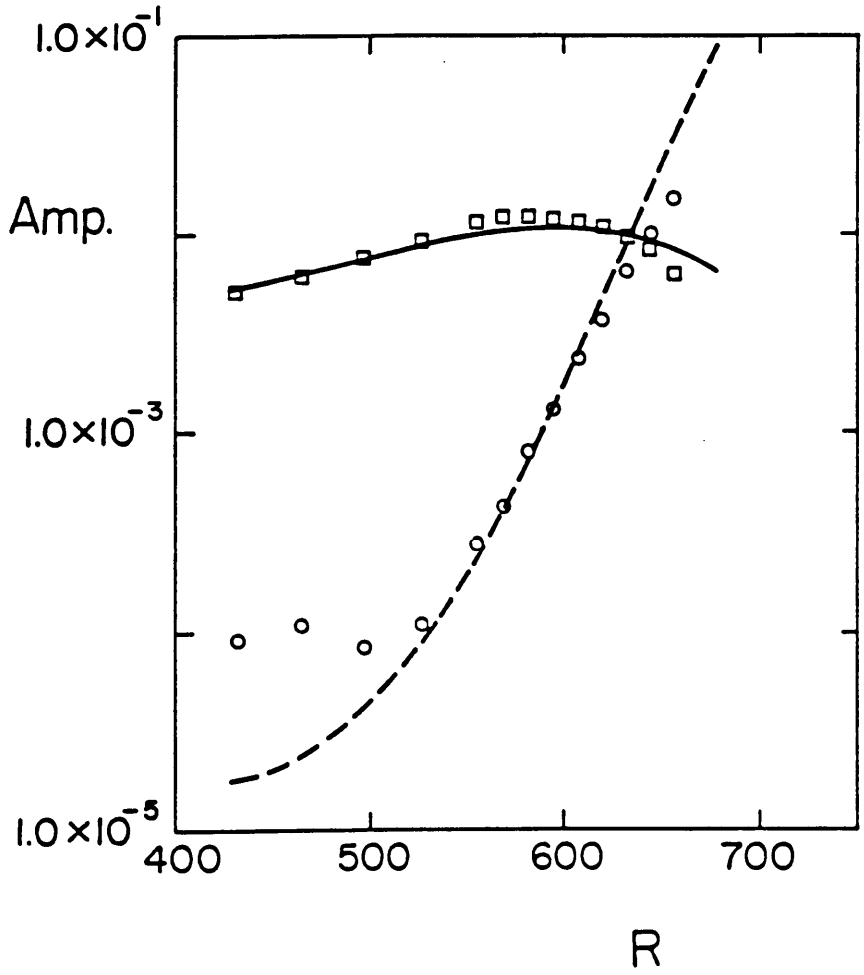

Figure 13. Variation with R of the r.m.s amplitudes of the 2-D (——) and the 3-D subharmonic (----) waves as predicted by the Floquet theory model. $F_{2D} = 124 \times 10^{-6}$ and b = 0.33. At R = 430 the r.m.s. amplitudes of the 2-D and the 3-D waves are, respectively, 5.2×10^{-3} and 2.63×10^{-5}. O and □ are the experimental points from Ref. 9. Measurements and computations are at y*/B.L. thickness = 0.26.

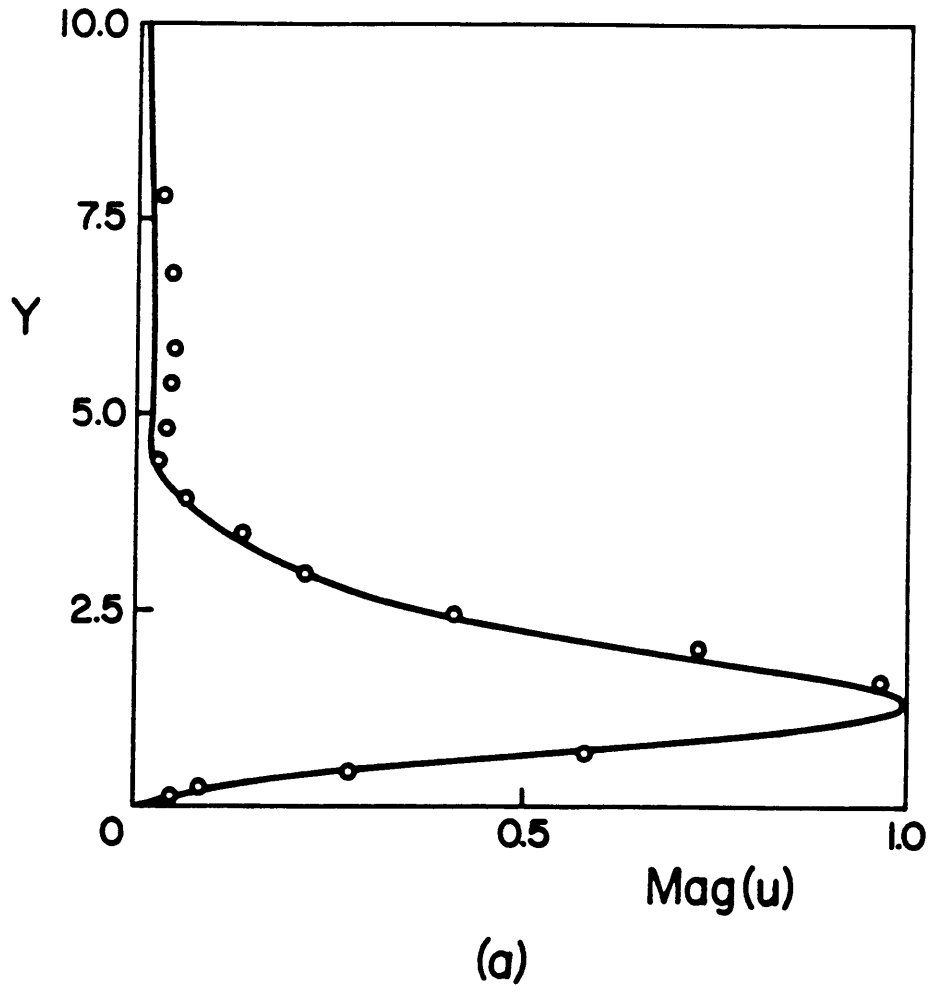

Figure 14. The y variation of the magnitude (a) and the phase (b) of the streamwise subharmonic disturbance at R = 606 as predicted by the Floquet theory model (——) compared with the experimental data (o) of Ref. 9. $F_{2D} = 124 \times 10^{-6}$ and b = 0.33. Experimental data are at R = 608.

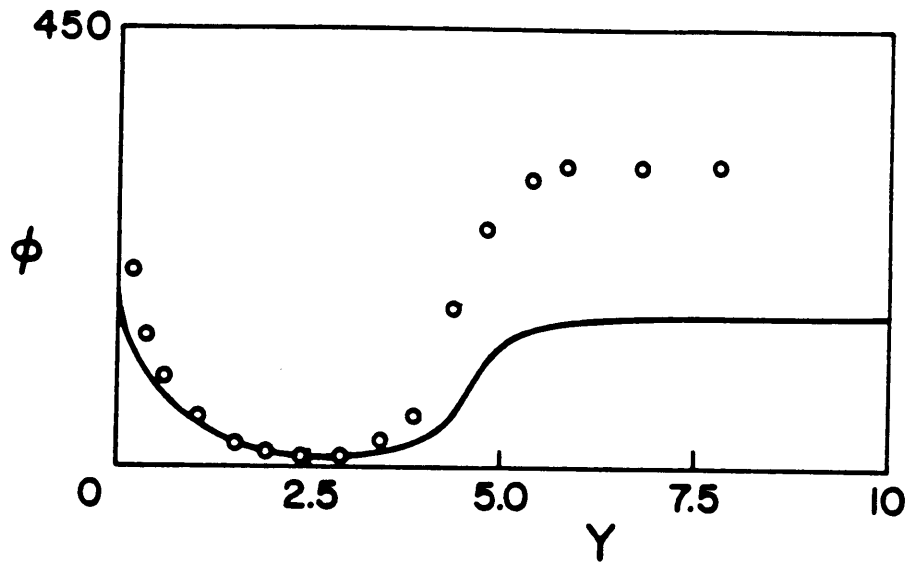

(b)

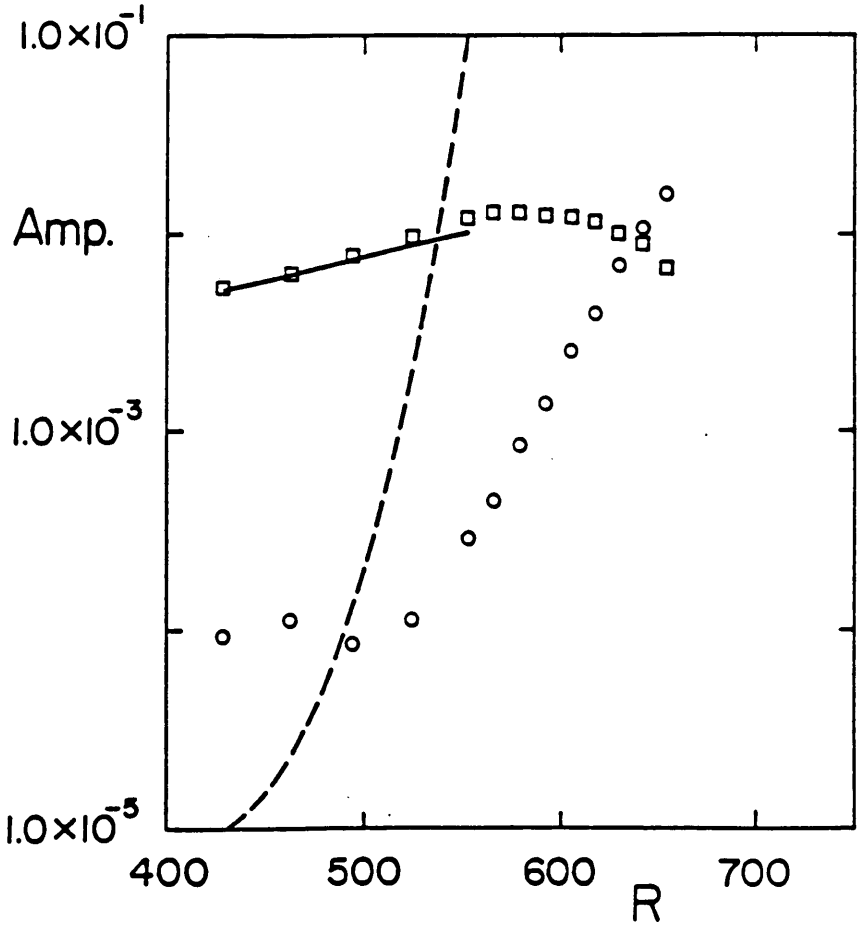

Figure 15. Variation with R of the r.m.s amplitudes of the 2-D (——) and the 3-D subharmonic (----) waves as predicted by the resonant triad model. $F_{2D} = 124 \times 10^{-6}$ and b = 0.33. At R = 430 the r.m.s. amplitudes of the 2-D and the 3-D waves are, respectively, 5.2×10^{-3} and 2.63×10^{-5}. O and □ are the experimental points from Ref. 9. Measurements and computations are at y*/B.L. thickness = 0.26.

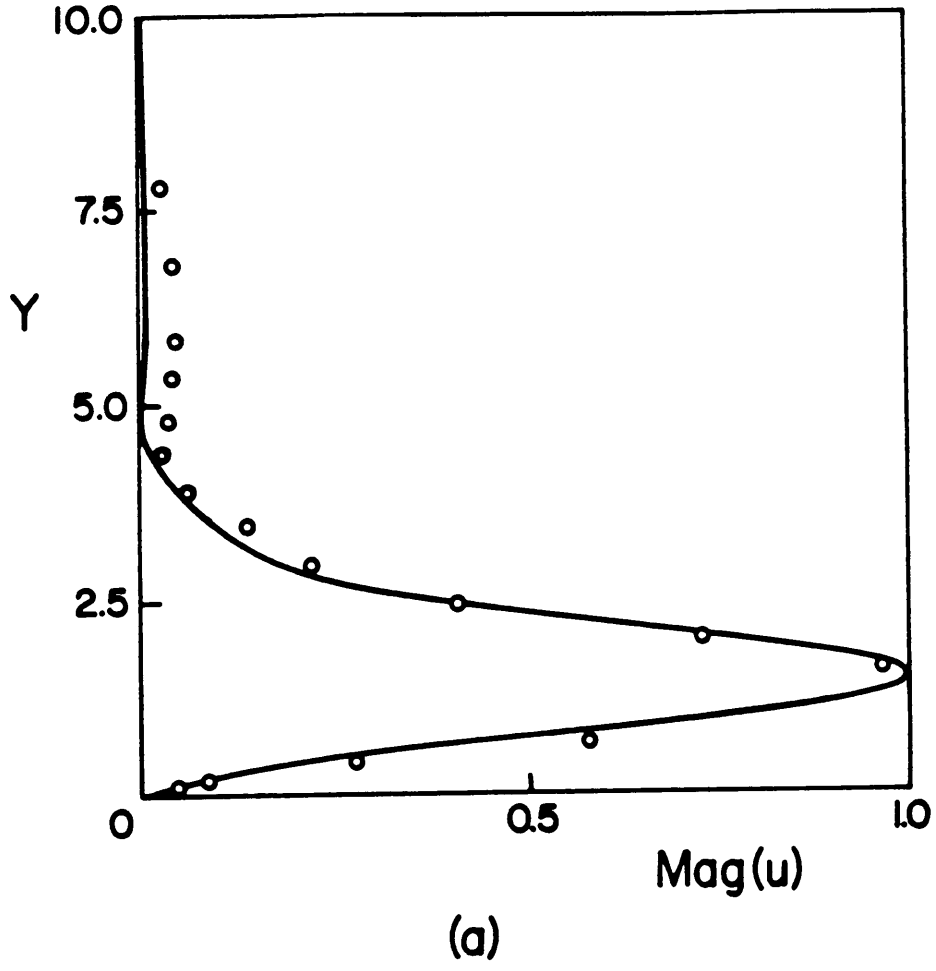

Figure 16. The y variation of the magnitude (a) and the phase (b) of the streamwise subharmonic disturbance at R = 606 as predicted by the resonant triad model (——) compared with the experimental data (o) of Ref. 9. $F_{20} = 124 \times 10^{-6}$ and b = 0.33. Experimental data is at R = 608.

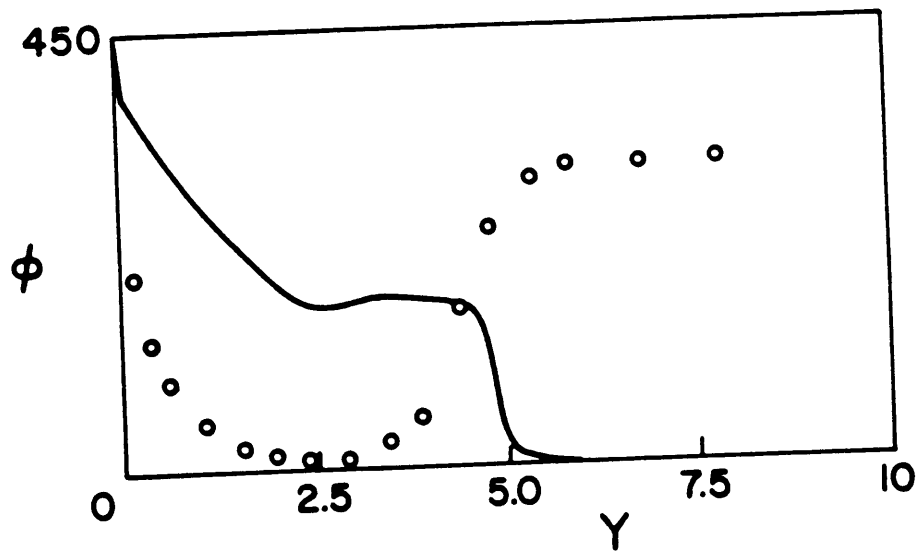

(b)

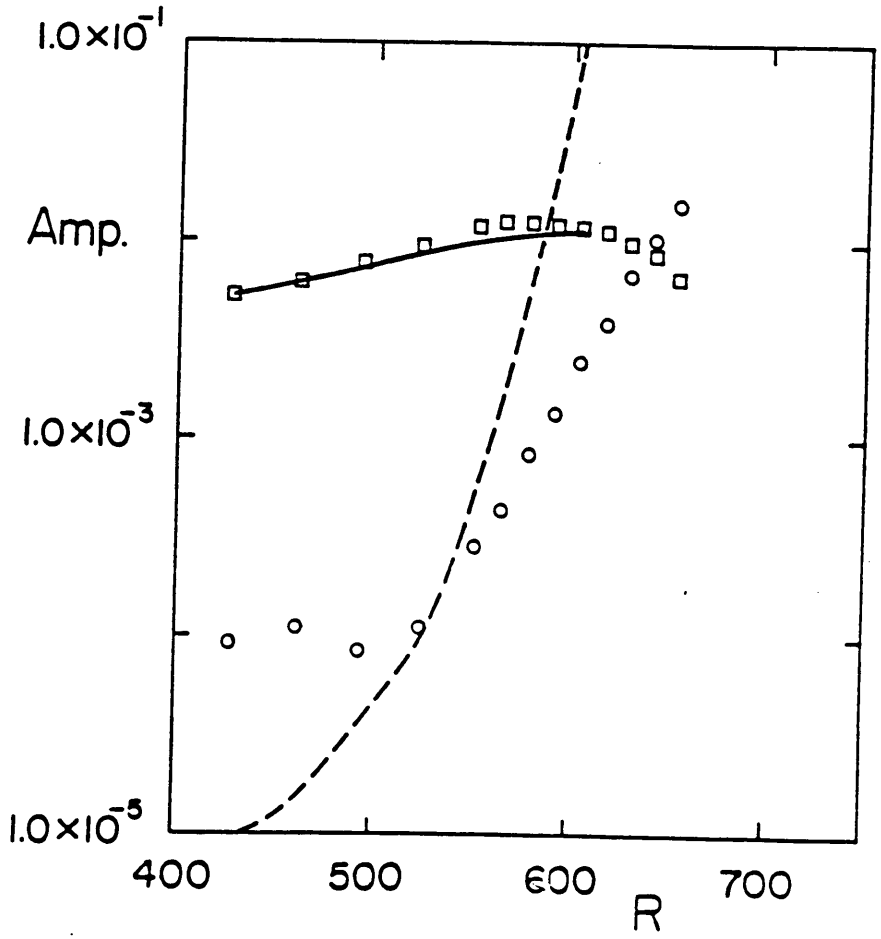

Figure 17. Variation with R of the r.m.s amplitudes of the 2-D (——) and the 3-D subharmonic (----) waves as predicted by the resonant triad model. $F_{2D} = 124 \times 10^{-6}$ and b = 0.18. At R = 430 the r.m.s. amplitudes of the 2-D and the 3-D waves are, respectively, 5.2×10^{-3} and 2.83×10^{-5}. O and □ are the experimental points from Ref. 9. Measurements and computations are at y*/B.L. thickness = 0.26.

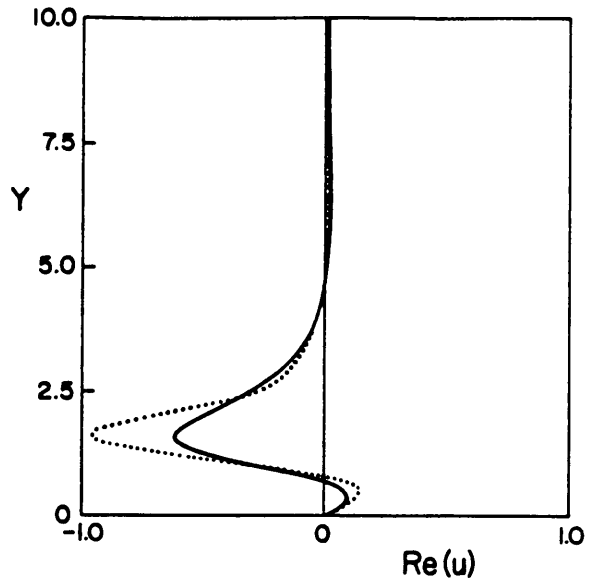

(a)

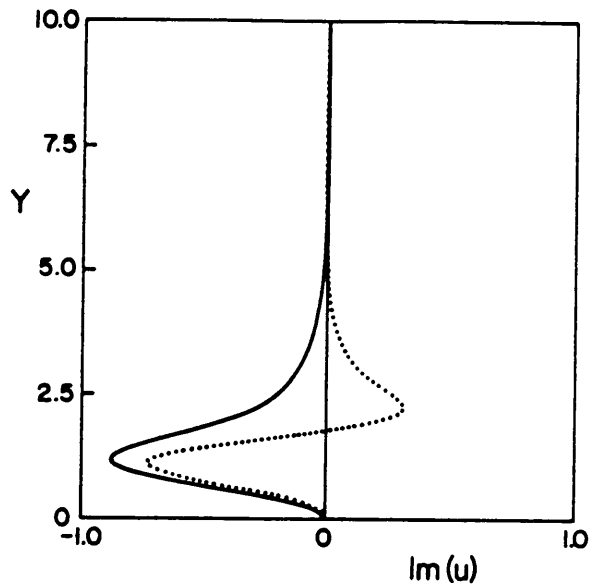

(b)

Figure 18. The y variation of the eigenfunctions of the subharmonic mode as predicted by the Floquet theory model (——) compared with the eigenfunctions of the 3-D T-S O-S mode (····). $F_{2D} = 124 \times 10^{-6}$, the r.m.s. amplitude of the 2-D wave is 0.0133, b = 0.33 and R = 606. a,b,c,d,e,f,g, and h are for ξ_{1r}, ξ_{1i}, ξ_{3r}, ξ_{3i}, ξ_{4r}, ξ_{4i}, ξ_{5r} and ξ_{5i}, respectively.

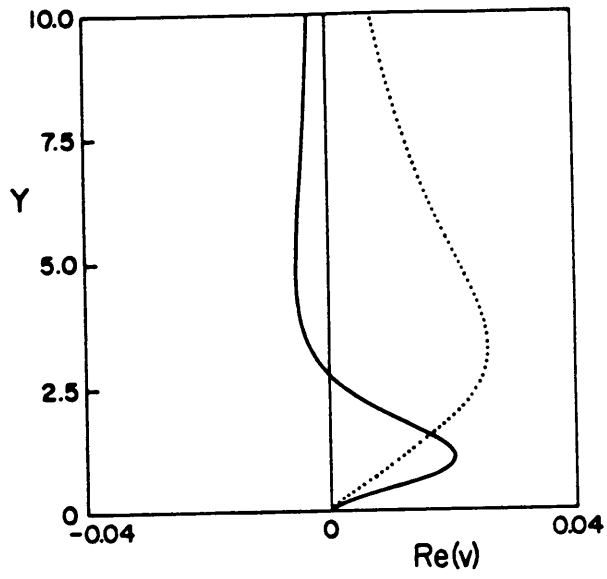

(c)

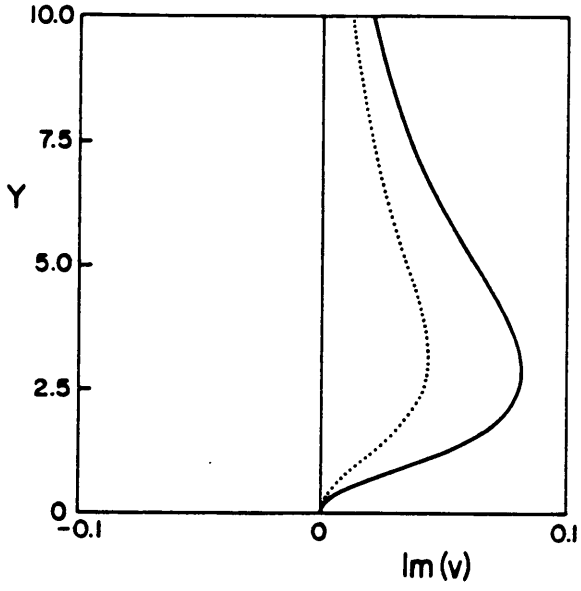

(d)

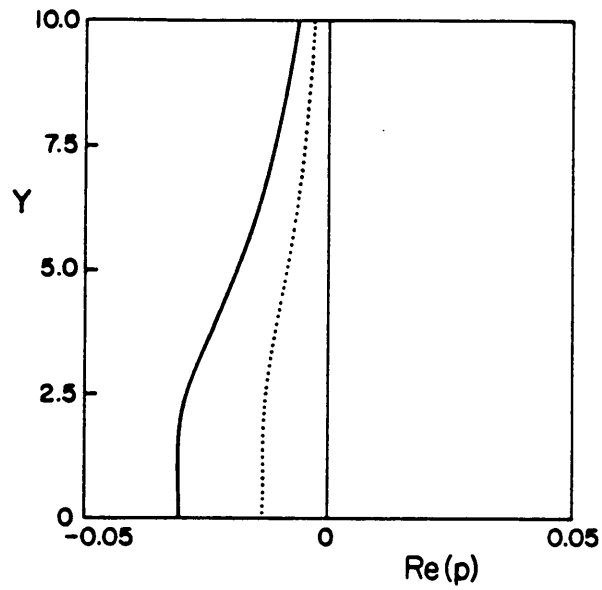

(e)

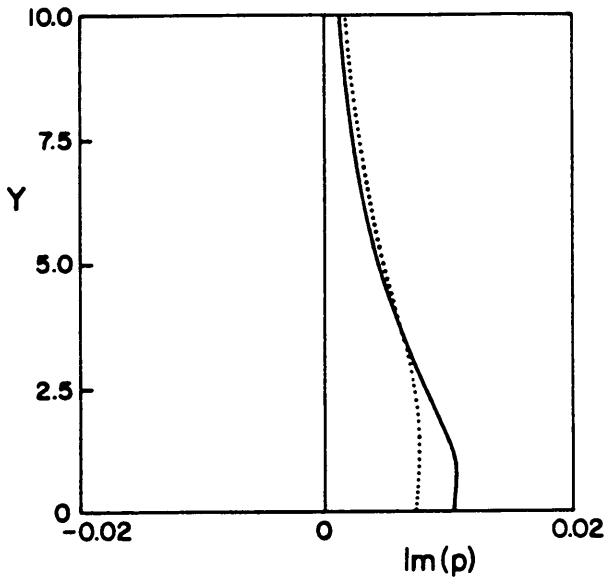

(f)

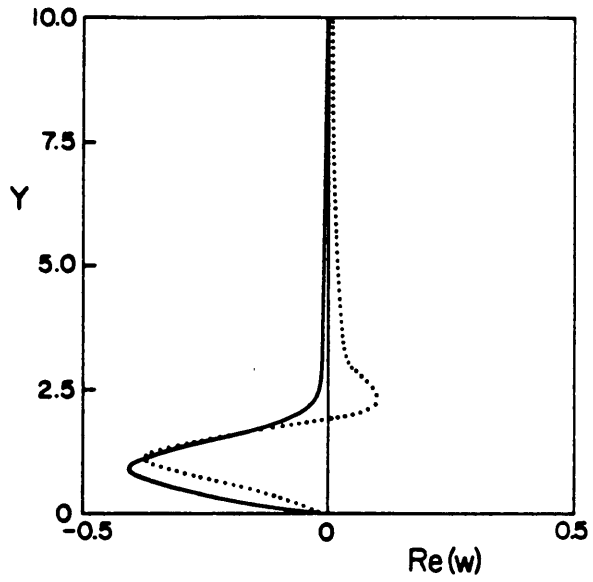

(g)

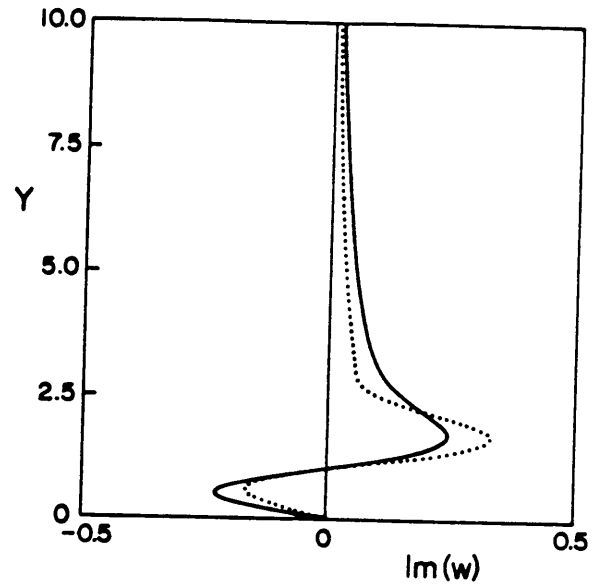

(h)

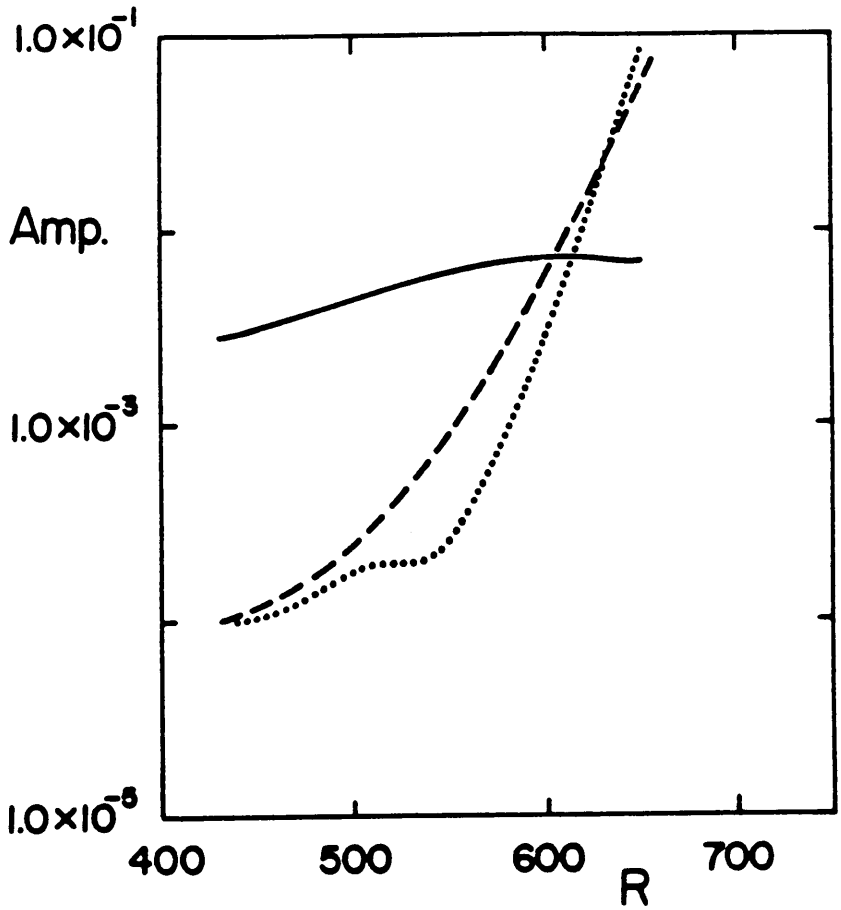

Figure 19. The variation with R of the maximum r.m.s. amplitudes of the 2-D (——) and the 3-D 0-S subharmonic predicted by the resonant triad (....) compared with the subharmonic predicted by the Floquet theory model (----). F_{2D} = $.124\times10^{-6}$, b = 0.18 and at R = 430 the r.m.s. amplitude of the 2-D is 2.86×10^{-3}.

The vita has been removed from the scanned document

ABSTRACT

The subharmonic instability in two-dimensional boundary layer on a flat plate is analyzed using the parametric instability model and the resonant triad model. The problems arising from both models are solved numerically using the shooting technique and results are presented. It is found that in the presence of a strong interaction (e.g., large amplitude of the two-dimensional wave), results from the resonant triad model are inaccurate as compared with the experimental data and the results from the parametric instability model. This is mainly because the resonant triad model is a weakly nonlinear model, and it does not account for the modification of the eigenfunctions of the interacting waves which really takes place as we find out from the experiments.

The parametric instability model is a powerful model, despite all the assumptions included. The model, however, does not introduce a clear understanding of how the subharmonic mode originates from the three-dimensional Tollmien-Schlichting modes.

For a weak interaction results from the resonant triad model and the parametric instability model get close to each other.